We are IntechOpen, the world's leading publisher of Open Access books Built by scientists, for scientists

4,800
Open access books available

122,000
International authors and editors

135M
Downloads

Our authors are among the

154
Countries delivered to

TOP 1%
most cited scientists

12.2%
Contributors from top 500 universities

CLARIVATE ANALYTICS BOOK CITATION INDEX INDEXED

WEB OF SCIENCE™

Selection of our books indexed in the Book Citation Index in Web of Science™ Core Collection (BKCI)

Interested in publishing with us?
Contact book.department@intechopen.com

Numbers displayed above are based on latest data collected.
For more information visit www.intechopen.com

14

Adaptive Control for Guidance of Underwater Vehicles

Mario Alberto Jordán and Jorge Luis Bustamante
Argentinian Institute of Oceanography (IADO-CONICET), National University of the South (UNS), Bahía Blanca Argentina

1. Introduction

Underwater vehicles are extensively employed in the offshore industry, subaquatic scientific investigations and rescue operations. They are sophisticated mechanisms with complex nonlinear dynamics and large lumped perturbations. They can remotely be operated or eventually autonomously navigate along specified scheduled trajectories with geometric and kinematic restrictions for obstacle avoidance or time-optimal operations (Fossen, 1994).

In a wide spectrum of applications, underwater vehicles are generally described by nonlinear and time-varying dynamics. For instance, dynamics with variable inertia and buoyancy arriving from sampling missions or hydrodynamics related to large changes of operation velocity or current perturbations in which laminar-to/from-turbulent transitions are involved in the hydrodynamics.

Due to the inherent nonlinear equations of motions, perturbed environments and complex missions, subaquatic vehicles require the guidance by means of complex controllers that usually involve automatic speed controls, dynamic positioning and tracking, and autopilot systems for automatic steering of depth and altitude. It is experimentally corroborated that adaptive techniques may provide superior trajectory tracking performance compared with the fixed model-based controllers (Smallwood & Whitcomb, 2003; 2004).

Many different adaptive and robust adaptive approaches for underwater vehicles have been discussed in the literature in the past 15 years to handle uncertainties related to the dynamics, hydrodynamics and external disturbances, see for instance Fossen & Fjellstad, 1995; Hsu et al., 2000, Antonelli et al., 2004; Wang & Lee, 2003; Do et al., 2004. However, the employment of novel high-performance nonlinear control design methodologies like backstepping (Krstić et al., 1995), passivity-based approaches (Fradkov et al., 1999) or sliding modes (Hsu et al., 2000) do not appear in the literature except as incipient applications, see for instance, Do & Pan, 2003; Li et al., 2004; Jordán & Bustamante, 2006; 2007; Conte & Serrani, 1999.

From previous theoretic results and some experimental corroborations, it seems that novel adaptive techniques can give rise to an improvement of the global performance in path tracking, above all when more precise manoeuvrability with a high celerity in motion is necessary in a changeable and uncertain subaquatic environment.

Source: Underwater Vehicles, Book edited by: Alexander V. Inzartsev,
ISBN 978-953-7619-49-7, pp. 582, December 2008, I-Tech, Vienna, Austria

In this chapter we present a general adaptive approach based on speed-gradient techniques that are modified for complex time-varying dynamics. Moreover, the dominant vehicle dynamics and hydrodynamics together with the often neglected thruster dynamics are considered in a complete time-varying and nonlinear model.
The chapter is organized as follows. First a description of the vehicle dynamics and hydrodynamics under environmental perturbations in 6 degrees of freedom is given. Additionally, thruster dynamics is described as embedded in the dominant dynamics like a fast dynamics (parasitics). Then, the tracking and regulation problems are introduced in a general form as minimization of a energy cost functional involving positioning and kinematic errors. Afterwards, a design of a fixed controller is presented. The same methodology is extended to the adaptive case. Then, an extension of the adaptive system structure by means of a state/disturbance observer is developed. Afterwards, global convergence of positioning and kinematic path errors is proved in form of theorem results. Finally, the analysis of a selected case study of navigation in a complex sampling mission illustrates the achievable high performance of the presented control approach.

2. Vehicle dynamics

We consider a Lagrangian approach for describing the vehicle dynamics in 6 degrees of freedom (Fossen, 1994). Moreover, we shall develop here an extension of the usual model for time-varying vehicle dynamics.

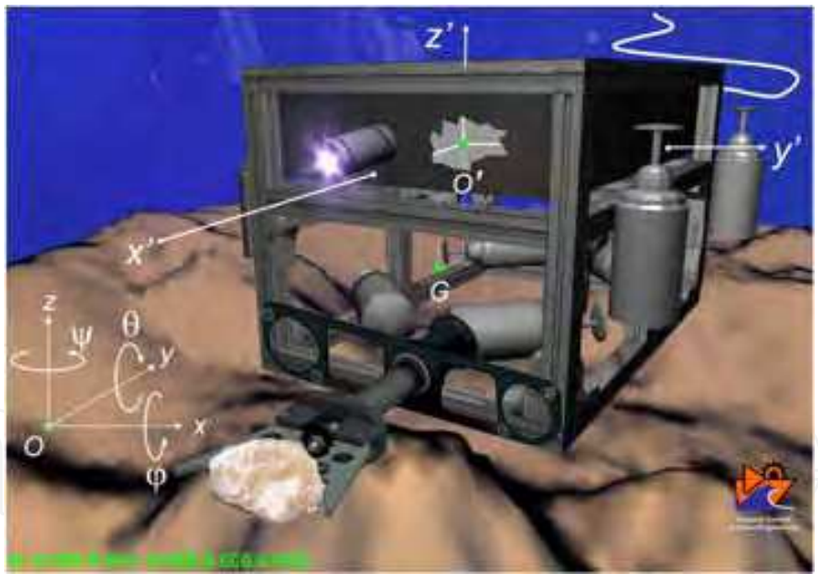

Fig. 1. Case study: full controllable underwater vehicle with 8 thrusters (MUM-TUHH, Hamburg, Germany) with manipulator

2.1 Time-varying dynamics

Consider the Fig. 1. and let us define the generalized position of the vehicle with respect to an earth-fixed frame. This is denoted by the vector $\boldsymbol{\eta} = [x, y, z, \varphi, \theta, \psi]^T$ indicating translations in the x direction (surge), in the y direction (sway), in the z direction (heave), and the so-called Euler angles: φ (roll) about the x axis, θ (pitch) about the y axis, and ψ

(yaw) about the z axis, respectively. Similarly, but referred to a body-fixed frame, the generalized velocity vector $\mathbf{v} = [u, v, w, p, q, r]^T$ indicates linear rates u, v, w, along the main vehicle axis x', y', z', respectively, and angular rates p, q, r, about the axis x', y', z', respectively.

The start point for dynamics description is the kinematic and potential energies of the vehicle, termed T and V, respectively. Consider besides the earth-fixed frame. So, the Lagragian is

$$L = T - V. \tag{1}$$

After applying the Lagragian equation it is valid particularly

$$\frac{d}{dt}\left(\frac{\partial L}{\partial \dot{\boldsymbol{\eta}}}\right) - \frac{\partial L}{\partial \boldsymbol{\eta}} + \frac{\partial P_d}{\partial \dot{\boldsymbol{\eta}}} = \boldsymbol{\tau}_\eta, \tag{2}$$

where $\boldsymbol{\tau}_\eta$ is the generalized force applied to the vehicle in some arbitrary point O' (not necessarily the mass center G, see Fig. 1) and P_d is the dissipated energy which is related to a drag force term through

$$\frac{\partial P_d}{\partial \dot{\boldsymbol{\eta}}} = D_\eta\left(\mathbf{v}, \boldsymbol{\eta}\right)\dot{\boldsymbol{\eta}}. \tag{3}$$

with D_η being the generalized drag matrix with respect to the earth-fixed frame. Moreover, the Lagragian is given by

$$L = T_{rb} + T_f - V, \tag{4}$$

where T_{rb} is the kinematic energy of the rigid body, T_f the kinematic energy of the fluid and V fulfills

$$\frac{\partial V}{\partial \boldsymbol{\eta}} = \mathbf{g}_\eta\left(\boldsymbol{\eta}\right), \tag{5}$$

with $\mathbf{g}_\eta$ being the generalized buoyancy force. Additionally, the total kinematic energy in (4) can be expressed as

$$T = T_{rb} + T_f = \frac{1}{2}\dot{\boldsymbol{\eta}}^T M_\eta\left(\boldsymbol{\eta}\right)\dot{\boldsymbol{\eta}}, \tag{6}$$

with M_η being the generalized inertia matrix with respect to the earth-fixed frame. Thus

$$\frac{\partial L}{\partial \dot{\boldsymbol{\eta}}} = M_\eta\left(\boldsymbol{\eta}\right)\dot{\boldsymbol{\eta}} - \frac{\partial V}{\partial \dot{\boldsymbol{\eta}}} = M_\eta\left(\boldsymbol{\eta}\right)\dot{\boldsymbol{\eta}} \tag{7}$$

$$\frac{d}{dt}\left(\frac{\partial L}{\partial \dot{\boldsymbol{\eta}}}\right) = M_\eta\left(\boldsymbol{\eta}\right)\ddot{\boldsymbol{\eta}} + \dot{M}_\eta\left(\boldsymbol{\eta}\right)\dot{\boldsymbol{\eta}}. \tag{8}$$

Employing (4), (6) and (5), one achieves

$$\frac{\partial L}{\partial \boldsymbol{\eta}} = \frac{\partial T}{\partial \boldsymbol{\eta}} - \frac{\partial V}{\partial \boldsymbol{\eta}} = \frac{1}{2}\dot{\boldsymbol{\eta}}^T \frac{\partial M(\boldsymbol{\eta})}{\partial \boldsymbol{\eta}}\dot{\boldsymbol{\eta}} - \mathbf{g}(\boldsymbol{\eta}). \tag{9}$$

Besides

$$\dot{M}_\eta(\boldsymbol{\eta}) = \dot{\boldsymbol{\eta}}^T \frac{\partial M_\eta(\boldsymbol{\eta})}{\partial \boldsymbol{\eta}}. \tag{10}$$

Finally, (2) can be written over again as

$$M_\eta(\boldsymbol{\eta})\ddot{\boldsymbol{\eta}} + \frac{1}{2}\dot{M}_\eta(\boldsymbol{\eta})\dot{\boldsymbol{\eta}} + D_\eta(\mathbf{v},\boldsymbol{\eta})\dot{\boldsymbol{\eta}} + \mathbf{g}_\eta(\boldsymbol{\eta}) = \boldsymbol{\tau}_\eta. \tag{11}$$

From this expression, one can recognize the generalized thrust force $\boldsymbol{\tau}_\eta$ and the so-called generalized matrix of the Coriolis and centripetal force given by

$$C_\eta(\mathbf{v},\boldsymbol{\eta}) = \frac{1}{2}\dot{M}_\eta(\boldsymbol{\eta}). \tag{12}$$

On the other side, the most appropriate form of the equation of motion is related to the body-fixed frame. In order for (11) to be expressed in this frame, let us consider the frame coordinate relation

$$\dot{\boldsymbol{\eta}} = J(\boldsymbol{\eta})\mathbf{v}, \tag{13}$$

where J is the rotation matrix (see Fossen, 1994) depending on the Euler angles θ and φ. The matrix J is not singular as long as the pitch angle fulfills $|\theta| < \pi/2$. So, with

$$\ddot{\boldsymbol{\eta}} = \frac{dJ(\boldsymbol{\eta})}{dt}\mathbf{v} + J(\boldsymbol{\eta})\dot{\mathbf{v}} \tag{14}$$

one obtains

$$\mathbf{v} = J^{-1}(\boldsymbol{\eta})\dot{\boldsymbol{\eta}} \tag{15}$$

$$\dot{\mathbf{v}} = J^{-1}(\boldsymbol{\eta})\ddot{\boldsymbol{\eta}} - J^{-1}\frac{dJ(\boldsymbol{\eta})}{dt}J^{-1}(\boldsymbol{\eta})\dot{\boldsymbol{\eta}}. \tag{16}$$

With (14) in (16) and comparing this result with (11), one can identify the matrices of the new dynamics description

$$M_\eta(\boldsymbol{\eta}) = J^{-T}(\boldsymbol{\eta})MJ^{-1}(\boldsymbol{\eta}) \tag{17}$$

$$C_\eta(\mathbf{v},\boldsymbol{\eta}) = J^{-T}(\boldsymbol{\eta})\left[C(\mathbf{v}) - MJ^{-1}(\boldsymbol{\eta})\frac{dJ(\boldsymbol{\eta})}{dt}\right]J^{-1}(\boldsymbol{\eta}) \tag{18}$$

$$D_\eta(\mathbf{v},\boldsymbol{\eta}) = J^{-T}(\boldsymbol{\eta})D(\mathbf{v}) \tag{19}$$

$$\mathbf{g}_\eta(\boldsymbol{\eta}) = J^{-T}(\boldsymbol{\eta})\mathbf{g}(\boldsymbol{\eta}) \tag{20}$$

$$\boldsymbol{\tau}_{\eta} \quad = \quad J^{-T}(\boldsymbol{\eta})\,\boldsymbol{\tau}_{t}, \tag{21}$$

with *M, C, D*, **g** and $\boldsymbol{\tau}_t$ being the generalized matrices and vectors accounting for the inertia matrix, the Coriolis and centripetal matrix, the drag matrix, the buoyancy and the thrust force, respectively, all them with respect to the body-fixed frame.
Replacing (17) of M_η in (10) of $\dot{M}_\eta$ and this result in (12) one accomplishes

$$C_{\eta}(\mathbf{v},\boldsymbol{\eta}) = \frac{1}{2}\left(\frac{dJ^{-T}(\boldsymbol{\eta})}{dt}MJ^{-1}(\boldsymbol{\eta}) + J^{-T}(\boldsymbol{\eta})\,\dot{M}J^{-1}(\boldsymbol{\eta}) + J^{-T}(\boldsymbol{\eta})\,M\frac{dJ^{-1}(\boldsymbol{\eta})}{dt}\right). \tag{22}$$

Now from (22) in (18) one obtains the final expression for the generalized matrix of Coriolis and centripetal force with respect to the body-fixed frame

$$C(t,\mathbf{v}) = \frac{1}{2}\left(J^{T}(\boldsymbol{\eta})\,\frac{dJ^{-T}(\boldsymbol{\eta})}{dt}M + \dot{M} + M\frac{dJ^{-1}(\boldsymbol{\eta})}{dt}J(\boldsymbol{\eta})\right) + MJ^{-1}(\boldsymbol{\eta})\,\frac{dJ(\boldsymbol{\eta})}{dt}. \tag{23}$$

It is noticing from (23) that the supposed time variance of the dynamics at the beginning of the section, leads to the appearance of the new term $\frac{1}{2}\dot{M}$ in comparison with the time invariant model in Fossen, 1994.
Finally, the dynamics of the time-varying dynamics of the underwater vehicle is described by two ordinary differential equations (ODEs)

$$\dot{\mathbf{v}} \quad = \quad M^{-1}(t)\left(-\left(C_c(t,\mathbf{v}) + \frac{1}{2}\dot{M}(t)\right)\mathbf{v} - D(t,\mathbf{v})\mathbf{v} - \mathbf{g}(t,\boldsymbol{\eta}) + \boldsymbol{\tau}_t\right) \tag{24}$$

$$\dot{\boldsymbol{\eta}} \quad = \quad J(\boldsymbol{\eta})\,\mathbf{v}. \tag{25}$$

where the time dependence in the systemmatrices is explicitly declared in the notation. Moreover, it is assumed the existence of $M^{-1}(t)$ uniformly in time, and C_c is the part of *C* in (23) that does not contain the term $\frac{1}{2}\dot{M}$.

2.2 System matrices description

In the following, a detailed description of expressions for the system matrices *M, C, D* and **g** will be given from a physical point of view.
The inertia matrix *M* can be decomposed into the so-called body inertia matrix M_b and the added mass matrix M_a which accounts for the surrounded fluid mass. So, it is valid

$$M(t) = M_b(t) + M_a(t). \tag{26}$$

The body inertia matrix is

$$M_b(t) \quad = \quad \begin{bmatrix} m(t) & 0 & 0 \\ 0 & m(t) & 0 \\ 0 & 0 & m(t) \\ 0 & -m(t)z_G(t) & m(t)y_G(t) \\ m(t)z_G(t) & 0 & -m(t)x_G(t) \\ -m(t)y_G(t) & m(t)x_G(t) & 0 \end{bmatrix} \tag{27}$$

$$\begin{bmatrix} 0 & m(t)z_G(t) & -m(t)y_G(t) \\ -m(t)z_G(t) & 0 & m(t)x_G(t) \\ m(t)y_G(t) & -m(t)x_G(t) & 0 \\ I_x(t) & -I_{xy}(t) & -I_{xz}(t) \\ -I_{yx}(t) & I_y(t) & -I_{yz}(t) \\ -I_{zx}(t) & -I_{zy}(t) & I_z(t) \end{bmatrix},$$

where m is the vehicle mass, I_{ij} are the inertia moments with respect to the main axis i, j and x_G, y_G and z_G are the coordinates that determine the distance between the mass center G and the coordinate frame center O'. On the other side, the added inertia matrix is

$$M_a = \left(m_{a_{ij}}(t)\right), \text{ for } i,\ j = 1, ..., 6, \tag{28}$$

where the elements m_{aij} are functions of time of the added mass in each simple and cross motion with respect to the body main axis. Additionally, the inertia matrix fulfills $M = M^T > 0$. Similarly, the Coriolis and centripetal matrix can be described by taking the body mass and the added mass effects separately

$$C(t, \mathbf{v}) = C_b(t, \mathbf{v}) + C_a(t, \mathbf{v}), \tag{29}$$

where

$$C_b(t, \mathbf{v}) = \begin{bmatrix} 0 & 0 & 0 \\ 0 & 0 & 0 \\ 0 & 0 & 0 \\ -m(t)\left(y_G(t)q + z_G(t)r\right) & m(t)\left(y_G(t)p + w\right) & m(t)\left(z_G(t)p - v\right) \\ m(t)\left(x_G(t)q - w\right) & -m(t)\left(z_G(t)r + x_G(t)p\right) & m(t)\left(z_G(t)q + u\right) \\ m(t)\left(x_G(t)r + v\right) & m(t)\left(y_G(t)r - u\right) & -m(t)\left(x_G(t)p + y_G(t)q\right) \end{bmatrix} \tag{30}$$

$$\begin{bmatrix} -m(t)\left(x_G(t)q - w\right) & -m(t)\left(x_G(t)r + v\right) & m(t)\left(y_G(t)q + z_G(t)r\right) \\ m(t)\left(z_G(t)r + x_G p\right) & -m(t)\left(y_G(t)r - u\right) & -m(t)\left(y_G(t)p + w\right) \\ -m(t)\left(z_G(t)q + u\right) & m(t)\left(x_G(t)p + y_G(t)q\right) & -m(t)\left(z_G(t)p - v\right) \\ -I_{yz}(t)q - I_{xz}(t)p + I_{zz}(t)r & I_{yz}(t)r + I_{xz}(t)p - I_{yy}(t)q & 0 \\ 0 & -I_{xz}(t)r - I_{xy}(t)q + I_{xx}(t)p & I_{yz}(t)q + I_{xz}(t)p - I_{zz}(t)r \\ I_{xz}(t)r + I_{xy}(t)q - I_{xx}(t)p & 0 & -I_{yz}(t)r - I_{xy}(t)p + I_{yy}(t)q \end{bmatrix}$$

$$C_a(t, \mathbf{v}) = \begin{bmatrix} 0 & 0 & 0 \\ 0 & 0 & 0 \\ 0 & 0 & 0 \\ 0 & -\sum_{i=1}^{6} m_{a_{3i}}(t)v_i & \sum_{i=1}^{6} m_{a_{2i}}(t)v_i \\ \sum_{i=1}^{6} m_{a_{3i}}(t)v_i & 0 & -\sum_{i=1}^{6} m_{a_{1i}}(t)v_i \\ -\sum_{i=1}^{6} m_{a_{2i}}(t)v_i & \sum_{i=1}^{6} m_{a_{1i}}(t)v_i & 0 \end{bmatrix} \tag{31}$$

$$\begin{bmatrix} 0 & -\sum_{i=1}^{6} m_{a_{3i}}(t)v_i & \sum_{i=1}^{6} m_{a_{2i}}(t)v_i \\ \sum_{i=1}^{6} m_{a_{3i}}(t)v_i & 0 & -\sum_{i=1}^{6} m_{a_{1i}}(t)v_i \\ -\sum_{i=1}^{6} m_{a_{2i}}(t)v_i & \sum_{i=1}^{6} m_{a_{1i}}(t)v_i & 0 \\ 0 & -\sum_{i=1}^{6} m_{a_{6i}}(t)v_i & \sum_{i=1}^{6} m_{a_{5i}}(t)v_i \\ \sum_{i=1}^{6} m_{a_{6i}}(t)v_i & 0 & -\sum_{i=1}^{6} m_{a_{4i}}(t)v_i \\ -\sum_{i=1}^{6} m_{a_{5i}}(t)v_i & \sum_{i=1}^{6} m_{a_{4i}}(t)v_i & 0 \end{bmatrix}.$$

Additionally, $C(t, \mathbf{v})$ can be expanded into a linear combination according to

$$C(t,\mathbf{v}) = \sum_{i=1}^{6} C_i(t). \times C_{v_i}(v_i), \tag{32}$$

where the operator ".×" stays for an element-by-element operation between matrices, C_{v_i} are matrices depending on each single rate $v_i \in \{u, v, w, p, q, r\}$ and C_i contains time-varying coefficients of m, I_{ij}, $m_{a_{ij}}$ and the coordinates of G. The matrices C_{v_i} are constructed from (30) and (31) searching for the elements with v_i only, for instance, $C_{v_1}(v_1) = C_u(u)$=[0 0 0 0 u u; 0 0 0 u 0 u; 0 0 0 u u 0; 0 u u 0 u u; u 0 u u 0 u; u u 0 u u 0], and similarly for $C_v(v)$ up to $C_r(r)$. In the same way, C_1=[0 0 0 0 $-m_{a_{31}}$ $m_{a_{21}}$; 0 0 0 $m_{a_{31}}$ 0 (m- $m_{a_{1i}}$); 0 0 0 - $m_{a_{21}}$ (-m+ $m_{a_{1i}}$) 0; 0 $-m_{a_{31}}$ $m_{a_{21}}$ 0 $-m_{a_{61}}$ $m_{a_{51}}$; $m_{a_{31}}$ 0 (m - $m_{a_{11}}$) $m_{a_{61}}$ 0 $-m_{a_{41}}$; - $m_{a_{21}}$ (-m + $m_{a_{11}}$) 0 $-m_{a_{51}}$ $m_{a_{41}}$ 0], and similarly for C_2 up to C_6.

For the drag matrix, a suitable characterization can be done by superposing a constant matrix D_l accounting for laminar fluid effects and a velocity-depending matrix D_q diag($|\mathbf{v}|$) accounting by turbulence effects of the hydrodynamics

$$D(t,|\mathbf{v}|) = D_l(t) + D_q(t)\,\mathrm{diag}(|\mathbf{v}|), \tag{33}$$

where the notation diag($|\mathbf{v}|$) means diag($|u|$,..., $|r|$).

Finally, the total buoyancy vector is described in details by

$$\mathbf{g}(t,\boldsymbol{\eta}) = \begin{bmatrix} (W(t) - W_w(t))\, s(\theta) \\ -(W(t) - W_w(t))\, c(\theta)\, s(\phi) \\ -(W(t) - W_w(t))\, c(\theta)\, c(\phi) \\ -(W(t)y_G(t) - W_w(t)y_B(t))\, c(\theta)c(\phi) + (W(t)z_G(t) - W_w(t)z_B(t))\, c(\theta)s(\phi) \\ (W(t)x_G(t) - W_w(t)x_B(t))\, c(\theta)c(\phi) + (W(t)z_G(t) - W_w(t)z_B(t))\, s(\theta) \\ -(W(t)x_G(t) - W_w(t)x_B(t))\, c(\theta)s(\phi) - (W(t)y_G(t) - W_w(t)y_B(t))\, s(\theta) \end{bmatrix}, \tag{34}$$

where $s(.)$= sin(.) and $c(.)$= sin(.), W is the vehicle weight and W_w its buoyancy and x_B, y_B and z_B represent the coordinates of the metacenter in the body-fixed frame. Finally $\mathbf{g}$ can be appropriately put into a linear combination as

$$\mathbf{g}(t,\boldsymbol{\eta}) = B_1(t)\mathbf{g}_1(\boldsymbol{\eta}) + B_2(t)\mathbf{g}_2(\boldsymbol{\eta}), \tag{35}$$

where

$$\mathbf{g}_1(\boldsymbol{\eta}) = [\sin\theta, \cos\theta\sin\phi, \cos\theta\cos\phi, \cos\theta\cos\phi, \cos\theta\cos\phi, \sin(\theta)]^T \tag{36}$$

$$\mathbf{g}_2(\boldsymbol{\eta}) = [0, 0, 0, \cos\theta\sin\phi, \sin\theta, \cos(\theta)\sin(\phi)] \tag{37}$$

$$\begin{aligned} B_1(t) = \mathrm{diag}\,(&W(t) - W_w(t), W(t) - W_w(t), W(t) - W_w(t), \\ &W(t)y_G(t) - W_w(t)y_B(t), W(t)x_G(t) - W_w(t)x(t)_B, \\ &W(t)y_G(t) - W_w(t)y_B(t)) \end{aligned} \tag{38}$$

$$B_2(t) = \begin{aligned} &\mathrm{diag}\,(0,0,0, W(t)z_G(t) - W_w(t)z_B(t), \\ &\quad W(t)z_G(t) - W_w(t)z_B(t), W(t)x_G(t) - W_w(t)x_B(t))\,. \end{aligned} \tag{39}$$

Clearly, B_1 and B_2 are matrices with time dependence due to changes in the weight, buoyancy, mass center and metacenter, while $\mathbf{g}_1$ and $\mathbf{g}_2$ are state-dependent vectors.

2.3 On the physical variability of the system parameters

The vehicle dynamics is usually subject to changes according to phenomenological and operation-dependent sources. Generally, for vehicles with high manoeuvrability, the hydrodynamics can change in the form of complex transitions from laminar to turbulent flow and vice versa in the wide range of $\mathbf{v}$ and currents. Moreover, in sampling missions over the sea bottom, the vehicle mass and its distribution in the vehicle is modified in a staggered form. Similarly, for fuel-propelled vehicles, there exists a continuous decreasing of the total mass during the navigation and also complex sloshing phenomena take place that modify the inertia properties in time.
For these scenarios, the inertia matrix can be modelled appropriately by

$$M(t) = M_c(t) + \sum_{k=1}^{n} \Delta M_k h(t - t_k), \tag{40}$$

where M_c is the bounded and continuous part of M and ΔM_k are the steps of sudden changes of M at discrete times $t_k \in \mathcal{S}_{t_k}$, with $k = 1, ..., n$, and $\mathcal{S}_{t_k}$ a set for discrete time points and h is the step function. Correspondingly, the derivative of M accomplishes

$$\dot{M}(t) = \dot{M}_c(t) + \sum_{k=1}^{n} \Delta M_k \delta(t - t_k), \tag{41}$$

with δ the delta function. Physically, the sudden changes ΔM_k accounts only for the mass of the vehicle and not for the surrounded fluid, i.e., only M_b but not M_a in (26) is modified.
The variations of M cause also changes in the Coriolis and centripetal matrix C, see (23), in the form of a piecewise continuous evolution in time, but also C is unbounded at time points $t_k \in \mathcal{S}_{t_k}$. Similarly as before, sudden changes of M only affect C_b of the rigid body in (29) but not C_a of the surrounded fluid. Finally, the buoyancy matrices B_1 and B_2 in (35) evolve bounded and piecewice continuous due to changes in (40).
On the other side, the drag matrices D_l and D_{q_i} in (33) are assumed, in a general form, variable in time, also bounded but continuous.

2.4 Existence and uniqueness of solutions

Let us consider again the vehicle dynamics described by the ODEs (24)-(25) and a period of continuity of $M(t)$, i.e., for $t \in [t_k, t_{k+1})$ with $i = 1, ..., n$ and $t_k \in \mathcal{S}_{t_k}$. Additionally let $\boldsymbol{\eta}(t_0) \in \mathcal{S}_\eta$ and $v(t_0) \in \mathcal{S}_v$ be initial conditions.
Since the force components $C_c\mathbf{v}$, $D\mathbf{v}$ and $\mathbf{g}$ are Lipschitz continuous in $\boldsymbol{\eta} \in \mathcal{S}_\eta$ and $\mathbf{v} \in \mathcal{S}_v$, with the matrices $M_c(t)$, $C_{c_i}(t)$, $D_l(t)$, $D_{q_i}(t)$, $B_1(t)$ and $B_2(t)$ being continuous in this period, and $\boldsymbol{\tau}_t(t)$ is generally piecewise continuous in the period considered, then there exists a new, in general, shorter period T where $\boldsymbol{\eta}(t)$ and $\mathbf{v}(t)$ also exist and are unique in $t \in [t_k, t_k+T) \subseteq$

$[t_k, t_{k+1})$ (see Theorem of Existence and Uniqueness, for instance, in O'Reagan, 1997; Vidyasagar, 1993).
It is clear that $\frac{1}{2}\dot{M}\ \mathbf{v}$ of C in (23) will cause a step in the solution for $\mathbf{v}$ at every $t_k \in \mathcal{S}_{t_k}$ equal to

$$\Delta\mathbf{v}(t_k) = \frac{1}{2}M^{-1}(t_k)\Delta M_k\mathbf{v}(t_k). \tag{42}$$

However, the solution for $\boldsymbol{\eta}$ is continuous Lipschitz as it can be deduced from (25).
Thus, assuming the existence and uniqueness of the solutions $\boldsymbol{\eta}(t)$ and $\mathbf{v}(t)$ in every period $[t_k, t_{k+1})$, the complete solution of the system in $[t_0, \infty]$ is obtained by the composition of all pieces with conditions $\mathbf{v}(t_k)$ at the beginning of every piece equal to

$$\mathbf{v}(t_k)=(I + \frac{1}{2}M^{-1}(t_k)\Delta M_k)\lim_{t\to t_k}\mathbf{v}(t), \tag{43}$$

where $\mathbf{v}(t)$ is the solution obtained in $[t_{k-1}, t_k)$. In all this argumentation, the assumption that $\boldsymbol{\eta} \in \mathcal{S}_\eta$ is made for avoiding singularities of J outside $\mathcal{S}_\eta$ is made for $\eta_5 = \theta = \pm\pi/2$.

3. Thruster dynamics

The generalized thrust $\boldsymbol{\tau}_t$ is applied on O' (see Fig. 1). This force is decomposed into the thruster forces f_j actuating along the thruster axial direction j. All together are described in the propulsion vector $\mathbf{f} = [f_1, f_2, ..., f_n]^T$. Equivalently to $\boldsymbol{\tau}_t$ applied on O', f generates the physical impulses along every thruster shaft for the vehicle motion. They are related by

$$\boldsymbol{\tau}_{t_i} = \mathbf{b}_i f_i = \begin{bmatrix} \cos(\psi_i)\cos(\theta_i) \\ \sin(\psi_i)\cos(\theta_i) \\ -\sin(\theta_i) \\ -\sin(\theta_i)\, a_{y_i} - \sin(\psi_i)\cos(\theta_i)\, a_{z_i} \\ \cos(\psi_i)\cos(\theta_i)\, a_{z_i} + \sin(\theta_i)\, a_{x_i} \\ \sin(\psi_i)\cos(\theta_i)\, a_{x_i} - \cos(\psi_i)\cos(\theta_i)\, a_{y_i} \end{bmatrix} f_i, \tag{44}$$

where a_{x_i}, a_{y_i} and a_{z_i} are coordinates of the thruster propeller i referred to O', θ_i is the angle of the axial direction with respect to y' (generally $\theta_i = 0°$ or $\theta_i = 90°$ for horizontal or vertical thrusters, respectively) and ψ_i is the angle of the axial direction with respect to z'. In vector form it is valid

$$\boldsymbol{\tau}_t = \sum_{i=1}^{n}\mathbf{b}_i f_i = B\mathbf{f}, \tag{45}$$

where B is the matrix containing the vectors $\mathbf{b}_i$ as columns, with $i = 1, ..., n$. The thruster dynamics is characterized as (see Healey, 1995; Pinto, 1996; Fossen, 1994)

$$\mathbf{f} = K_1(|\mathbf{n}|.\mathbf{n}) - K_2(|\mathbf{n}|.\mathbf{v}_a) \tag{46}$$

$$\mathbf{n} = \mathbf{n}_1 + \mathbf{n}_2 \tag{47}$$

$$\mathbf{n}_1 = G_1(s)\,\mathbf{f} \tag{48}$$

$$\mathbf{n}_2 = G_2(s)\,\mathbf{u}_a \tag{49}$$

$$\mathbf{u}_a = G_{PID}(s)(\mathbf{n}_r - \mathbf{n}), \tag{50}$$

where $\mathbf{n}$ is the shaft rate vector, $\mathbf{n}_r$ is the reference of the rpm rate for $\mathbf{n}$, $\mathbf{v}_a$ is the vector with the axial velocities of the thrusters, $\mathbf{u}_a$ is the vector of the armature voltages for each DC motor, $\mathbf{n}_1$, $\mathbf{n}_2$ are auxiliary vectors, the operation ($\mathbf{x}.\mathbf{y}$) represents a new vector obtained by an element-by-element product, and similarly $|\mathbf{n}|$ represents a vector with elements $|n_i|$. The factors K_1 and K_2 in (46) are diagonal gain matrices describing the non-linear characteristic (see Fig. 2), G_1 and G_2 represents diagonal matrices with strictly proper Laplace transfer functions, and similarly, G_{PID} is a diagonal matrix with Laplace transfer functions representing an usual tachometric PID control loop of the DC motors.
Finally, the relation between the thruster output $\mathbf{n}$ and its reference $\mathbf{n}_r$ and the propulsion $\mathbf{f}$ is

$$\mathbf{n} = \frac{G_{PID}(s)G_2(s)}{I + G_{PID}(s)G_2(s)}\mathbf{n}_r + \frac{G_1(s)}{I + G_{PID}(s)G_2(s)}\mathbf{f}. \tag{51}$$

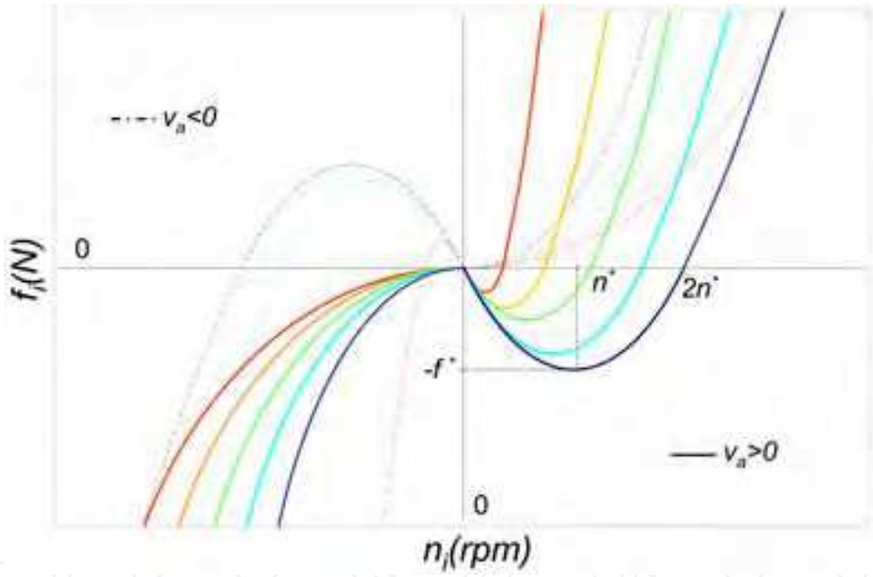

Fig. 2. Static Thruster characteristic

As $\boldsymbol{\tau}_t$ is actually the desired control action calculated by some guidance controller, the relation of it with the actuator thrust is also a desired propulsion referred to as

$$\mathbf{f}_{ideal} = B^T \left(BB^T\right)^{-1} \boldsymbol{\tau}_t. \tag{52}$$

In order to reach $\mathbf{f}_{ideal}$, the true f is provided by inputting n_r in (51) to the actuators. This will require the knowledge of $\mathbf{n}$ which is supposed here a non-measurable vector. So, an observer for $\mathbf{n}_r$, $\mathbf{n}$ and $\mathbf{f}$ will be employed later that uses $\mathbf{f}_{ideal}$ and the knowledge of the thruster model to perform the estimations.
Sometimes, the thruster dynamics can be modelled as parasitics in comparison to the dominant vehicle dynamics and consequently be simplified. A typical case of parasitics is

described by vehicles with large inertia for instance. In this case, making $s \rightarrow 0$ in (51) one accomplishes $\mathbf{n} = \mathbf{n}_r$ and clearly the thruster is described only by its static characteristic (46) of the Fig. 2. Additionally, using $\mathbf{f}_{ideal}$ and $\mathbf{v}_a$ in (46), $\mathbf{n}_r$ is determined if K_1 and K_2 are known. So, no observer is needed in this case to estimate $\mathbf{f}$ since $\mathbf{f} = \mathbf{f}_{ideal}$.

4. Servo-tracking problem

4.1 Asymptotic path tracking

The path tracking problem for the navigation system is introduced for two reference trajectories $\boldsymbol{\eta}_r(t)$ and $\mathbf{v}_r(t) = J^{-1}(\boldsymbol{\eta}_r)\,\dot{\boldsymbol{\eta}}_r$, which are uniformly continuous. Moreover let $\boldsymbol{\eta}(t)$ and $\mathbf{v}(t)$ be measured vectors that fulfills $\boldsymbol{\eta} \in \mathcal{S}_\eta = \{ x, y, z, \varphi, \psi \in \mathcal{R}^1, |\theta| < \pi/2\}$ and $\mathbf{v} \in \mathcal{S}_v \subset \mathcal{R}^6$. The specifications for the servo-tracking system are

$$\boldsymbol{\eta}(t) - \boldsymbol{\eta}_r(t) \rightarrow \mathbf{0}, \text{ for } t \rightarrow \infty \tag{53}$$

$$\mathbf{v}(t) - \mathbf{v}_r(t) \rightarrow \mathbf{0}, \text{ for } t \rightarrow \infty \tag{54}$$

for arbitrary initial conditions $\boldsymbol{\eta}(0) \in \mathcal{S}_\eta$, $\mathbf{v}(0) \in \mathcal{S}_v$. The sets $\mathcal{S}_\eta$ and $\mathcal{S}_v$ describe working regions of stability. Particularly, $\mathcal{S}_\eta$ characterizes the region where $J(\boldsymbol{\eta})$ is non singular (cf. (13) and description below it).

The way to keep spacial and kinematic vehicle trajectories close to their references is achieved by manipulating conveniently the thrust $\mathbf{f}$ by means of a control system. As introduced before, we focus in this work the design of an adaptive control system to achieve this goal.

To this end, let us define first a convenient expression to take account of the positioning and kinematic errors as (Conte & A. Serrani, 1999)

$$\tilde{\boldsymbol{\eta}} = \boldsymbol{\eta} - \boldsymbol{\eta}_r \tag{55}$$

$$\tilde{\mathbf{v}} = \mathbf{v} - J^{-1}(\boldsymbol{\eta})\dot{\boldsymbol{\eta}}_r + J^{-1}(\boldsymbol{\eta}) K_p \tilde{\boldsymbol{\eta}}, \tag{56}$$

with the gain matrix $K_p = K_p^T \geq 0$. Clearly, from (55)-(56) if $\tilde{\boldsymbol{\eta}}$ is zero with (25), it is valid $\tilde{\mathbf{v}} = \mathbf{v}(t) - \mathbf{v}_r(t)$.

Accordingly, from (24)-(25) with (55)-(56) one obtains the path error system

$$\dot{\tilde{\boldsymbol{\eta}}} = -K_p \tilde{\boldsymbol{\eta}} + J(\boldsymbol{\eta})\tilde{\mathbf{v}} \tag{57}$$

$$\begin{aligned} M\dot{\tilde{\mathbf{v}}} = & -C(\mathbf{v})\,\mathbf{v} - D(|\mathbf{v}|)\mathbf{v} + \mathbf{F}_b(\boldsymbol{\eta}) + \mathbf{F}_c + \mathbf{F}_t - M\frac{d}{dt}\left(J^{-1}(\boldsymbol{\eta})\dot{\boldsymbol{\eta}}_r\right) + \\ & + M\left(\frac{dJ^{-1}(\boldsymbol{\eta})}{dt}K_p - J^{-1}(\boldsymbol{\eta})K_p^2\right)\tilde{\boldsymbol{\eta}} + MJ^{-1}(\boldsymbol{\eta})K_p J(\boldsymbol{\eta})\tilde{\mathbf{v}}. \end{aligned} \tag{58}$$

Now, we will employ a speed-gradient technique to solve the path tracking problem asymptotically.

4.2 Controller design

The design of speed-gradient controllers starts with the definition of an energy cost functional of the state error vectors $\tilde{\boldsymbol{\eta}}$ and $\tilde{\mathbf{v}}$, which must be constructed as a radially unbounded and nonnegative scalar function (Fradkov et al., 1999). Accordingly, we propose

$$Q(\tilde{\boldsymbol{\eta}}, \tilde{\mathbf{v}}) = \frac{1}{2}\tilde{\boldsymbol{\eta}}^T\tilde{\boldsymbol{\eta}} + \frac{1}{2}\tilde{\mathbf{v}}^T M\tilde{\mathbf{v}}, \tag{59}$$

where Q results piecewise continuous due to the properties of M in time (see Section 2.3).
For an asymptotic stable controlled dynamics it is aimed that for every initial vectors $\boldsymbol{\eta}(0) \in \mathcal{S}_\eta$, $\mathbf{v}(0) \in \mathcal{S}_v$, it is valid from (59) and (53)-(54)

$$Q(\tilde{\boldsymbol{\eta}}(t), \tilde{\mathbf{v}}(t)) \to 0, \text{ for } t \to \infty. \tag{60}$$

According to the speed-gradient method (SG) (Fradkov et al., 1999), the manipulated variable $\boldsymbol{\tau}_t$ has to be build up in that way that $\dot{Q}$ be smooth, bounded and radially decreasing in the error space $\mathcal{S}_{\tilde{\eta}} \times \mathcal{S}_{\tilde{v}}$, and convex in the space of the controller parameters. For the time-varying conditions of the dynamics stated here, $\dot{Q}(t)$ does not fulfills the conditions of continuity because of $M(t)$ in (40).
So, we can analyze $Q(t)$ in the periods of continuity of the trajectory, it is for $t \in [t_0, \infty) \backslash \mathcal{S}_{t_k}$.
Combining (57)-(58), (55)-(56) with (59) and stating the first derivative of $Q(t)$ one obtains

$$\begin{aligned}\dot{Q}(t, t_0, \boldsymbol{\eta}_0, \mathbf{v}_0) = &-\tilde{\boldsymbol{\eta}}^T K_p\tilde{\boldsymbol{\eta}} + \tilde{\boldsymbol{\eta}}^T J(\boldsymbol{\eta})\tilde{\mathbf{v}} - \tilde{\mathbf{v}}^T C_c(t, \mathbf{v})\,\mathbf{v} - \tilde{\mathbf{v}}^T D_l(t)\mathbf{v} - \\ &-\tilde{\mathbf{v}} D_q(t, |\mathbf{v}|)\,\mathbf{v} - \tilde{\mathbf{v}}^T \mathbf{g}(t, \boldsymbol{\eta}) - \tilde{\mathbf{v}}^T M(t)\,\mathbf{d}(t, \tilde{\boldsymbol{\eta}}, \tilde{\mathbf{v}}) - \\ &-\tilde{\mathbf{v}}^T \frac{\dot{M}_c(t)}{2}\mathbf{v} + \tilde{\mathbf{v}}^T \frac{\dot{M}_c(t)}{2}\tilde{\mathbf{v}} + \tilde{\mathbf{v}}^T\boldsymbol{\tau}_c + \tilde{\mathbf{v}}^T\boldsymbol{\tau}_t\,,\end{aligned} \tag{61}$$

with

$$\mathbf{d}(t, \tilde{\boldsymbol{\eta}}, \tilde{\mathbf{v}}) = \frac{d}{dt}(J^{-1}(\boldsymbol{\eta})\dot{\boldsymbol{\eta}}_r) - \frac{dJ^{-1}(\boldsymbol{\eta})}{dt}K_p\tilde{\boldsymbol{\eta}} + J^{-1}(\boldsymbol{\eta})K_p^2\tilde{\boldsymbol{\eta}} - J^{-1}(\boldsymbol{\eta})K_p J(\boldsymbol{\eta})\tilde{\mathbf{v}}. \tag{62}$$

With the criterion of eliminating terms with undefined signs in (61) and so achieving the desired properties for $\dot{Q}(t)$, it can be deduced that the following control action is optimal in this sense

$$\begin{aligned}\boldsymbol{\tau}_t(t) = &\sum_{i=1}^{6} U_i \cdot \times C_{v_i}(v_i)\mathbf{v} + U_7\mathbf{v} + \sum_{i=1}^{6} U_{i+7}\,|v_i|\,\mathbf{v} + \\ &+U_{14}\mathbf{g}_1 + U_{15}\mathbf{g}_2 + U_{16}\mathbf{d} + U_{17}\tilde{\mathbf{v}} - K_v\tilde{\mathbf{v}} - J^T\tilde{\boldsymbol{\eta}} - \boldsymbol{\tau}_c\,,\end{aligned} \tag{63}$$

where the $\boldsymbol{U}_i$'s are matrices of the controller, C_{v_i} are the system matrices indicated in (32), $\mathbf{g}_1$ and $\mathbf{g}_2$ are the vectors defined in (36) and (37), and finally K_v is a new design matrix involving in the energy of the kinematic errors that accomplishes $K_v = K_v^T \geq 0$.
It is noticing that the cable force $\boldsymbol{\tau}_c$ here is supposed to be measurable and employed directly in the compensation in (63). Moreover, it is important to stress that the $\boldsymbol{U}_i$'s will have the

same structure of null and non-null elements as C_{c1}, ..., C_{c6}, (D_l-$\dot{M}_c$ /2), D_{q1}, ..., D_{q6}, B_1, B_2, M, and $\dot{M}_c$ have, respectively for i = 1, ..., 17. Thus, the number of elements in $\boldsymbol{U}_i$ can be reduced to a minimum considering the system matrix structure. In fact, one simple fixed controller (denoted by U_i^*) could be designed subject to the knowledge of a true dynamics model as

$$U_i^*(t) = C_{c_i}(t), for\ i = 1, ...6 \tag{64}$$

$$U_7^*(t) = D_l(t) + \frac{1}{2}\dot{M}_c(t) \tag{65}$$

$$U_i^*(t) = D_{q_i}(t), for\ i = 8, ...13 \tag{66}$$

$$U_{14}^*(t) = B_1(t) \tag{67}$$

$$U_{15}^*(t) = B_2(t) \tag{68}$$

$$U_{16}^*(t) = M(t) \tag{69}$$

$$U_{17}^*(t) = -\frac{1}{2}\dot{M}_c(t)\ . \tag{70}$$

Besides, the vector function candidate $\boldsymbol{\tau}_t$ ($\boldsymbol{U}_i$) in (63) must be such one that Q result convex in the controller parameters in the $\boldsymbol{U}_i$'s. It can be verified from (61)-(62) with (63) that this requirement is in fact satisfied.

4.3 Adaptive controller

Since the system dynamics is unknown, let the controller matrices $\boldsymbol{U}_i$'s be defined adaptively based on speed-gradient laws. Thus, introducing (63) in (61)-(62), it is defined

$$\dot{U}_i = -\Gamma_i \frac{\partial \dot{Q}(U_i)}{\partial U_i},\ \text{for}\ t \in [t_0, \infty) \backslash \mathcal{S}_{t_k}, \tag{71}$$

with $\Gamma_i = \Gamma_i^T > 0$ constant gain matrices for tuning the adaptation speed in each component $\boldsymbol{U}_i$ of $\boldsymbol{\tau}_t$. These laws allow to obtained $\boldsymbol{U}_i$'s as integral solutions of (71).
Particularly, for the Coriolis and centripetal matrix in its component C_c and its decomposition $C_{c_i}.\times C_{v_i}$ as in (32), it is found for the $\boldsymbol{U}_i$'s with i = 1, ..., 6

$$\dot{U}_i = -\Gamma_i \left(\hat{\mathbf{v}}\mathbf{v}^T\right).\times C_{v_i}(v_i). \tag{72}$$

Then, for the linear drag component D_l in (33) the law is applied as

$$\dot{U}_7 = -\Gamma_7 \hat{\mathbf{v}}\ \hat{\mathbf{v}}^T. \tag{73}$$

Analogously, for the quadratic drag component of D_q in (33) for the $\boldsymbol{U}_i$'s with i = 8, ..., 13, one achieves

$$\dot{U}_i = -\Gamma_i \hat{\mathbf{v}} \mathbf{v}^T |v_{i-7}|, \tag{74}$$

where v_i is the i-th element of $\mathbf{v}$.
Similarly, for the buoyancy matrices (38) and (39) in (35) it is obtained

$$\dot{U}_{14} = -\Gamma_{14} \hat{\mathbf{v}} \mathbf{g}_1^T \tag{75}$$

$$\dot{U}_{15} = -\Gamma_{15} \hat{\mathbf{v}} \mathbf{g}_2^T. \tag{76}$$

Next, for the inertia matrix M following law is assigned

$$\dot{U}_{16} = -\Gamma_{16} \hat{\mathbf{v}} \mathbf{d}^T, \tag{77}$$

where $\mathbf{d}$ is the auxiliary vector in (62).
Finally, for the unbounded Coriolis and centripetal component $\frac{1}{2}\dot{M}_c$, one gets

$$\dot{U}_{17} = -\Gamma_{17} \hat{\mathbf{v}} \hat{\mathbf{v}}^T. \tag{78}$$

The integration of the adaptive laws (72)-(78) with $\boldsymbol{U}_i(t_0) \in \mathcal{S}_U \subset \Re^{6\times 6}$, for i = 1, ..., 17, with $\mathcal{S}_U$ being a compact set, provides a direct calculation of the control action for the path tracking problem without knowledge about the variable system dynamics.

4.4 Modified adaptive laws

With the goal of obtaining a-priori bounded and smooth matrices $\boldsymbol{U}_i(t)$'s, we shall modify (71) with a smooth dynamic projection of the controller matrices (Pomet & Praly, 1992) on every column vector j of $\boldsymbol{U}_i$ referred to as $\mathbf{u}_{ij}$ in the following. Thus, the new $\boldsymbol{U}_i$'s are restrained to

$$\dot{\mathbf{u}}_{ij} = Proy\left(-\left(\Gamma_i \frac{\partial \dot{Q}}{\partial U_i}\right)_j\right) = \begin{cases} \left(-\Gamma_i \frac{\partial \dot{Q}}{\partial U_i}\right)_j, \text{ for } \mathbf{u}_{ij} \in \bar{M}_u \text{ or} \\ \left(\nabla_{u_{ij}} \mathcal{P}\right)^T \left(-\Gamma_i \frac{\partial \dot{Q}}{\partial U_i}\right)_j \leq 0 \\ (I - c(\mathbf{u}_{ij}) \Lambda \frac{\nabla_{u_{ij}} \mathcal{P} \nabla_{u_{ij}} \mathcal{P}^T}{\nabla_{u_{ij}} \mathcal{P} \Lambda \nabla_{u_{ij}} \mathcal{P}^T}) \left(-\Gamma_i \frac{\partial \dot{Q}}{\partial U_i}\right)_j, \text{ for} \\ \mathbf{u}_{ij} \in M_{u+\varepsilon} \backslash \bar{M}_u \text{or } \left(\nabla_{u_{ij}} \mathcal{P}\right)^T \left(-\Gamma_i \frac{\partial \dot{Q}}{\partial U_i}\right)_j \leq 0 \end{cases} \tag{79}$$

with

$$c(\mathbf{u}_{ij}) = \min\left\{1, \frac{\mathcal{P}(\mathbf{u}_{ij})}{\varepsilon}\right\}, \tag{80}$$

where $Proy(.)$ denotes the operator of the dynamic projection, additionally $(.)_j$. refers to the column j of the matrix in parenthesis, $\mathcal{P}$ is a convex function in the parametric space of $\mathbf{u}_{ij}$ and is specified in the convex set $M_{u+\varepsilon} = \{\mathbf{u}_{ij} \in \mathcal{R}^6 / \mathcal{P}(\mathbf{u}_{ij}) \leq \varepsilon\}$ composed by the union $M_u = \{\mathbf{u}_{ij} \in \mathcal{R}^6 / \mathcal{P}(\mathbf{u}_{ij}) \leq 0\}$ and the surrounding boundary $M_{u+\varepsilon} \backslash M_u$ with thickness $\varepsilon > 0$, arbitrary small. So $\bar{M}_u$ is the interior of M_u, ∂M_u is the contour of M_u and $\partial M_{u+\varepsilon}$ is the external contour of $M_{u+\varepsilon}$, both supposed smooth. Finally, Λ is a matrix that fulfills $\Lambda = \Lambda^T > 0$.

For future developments of the adaptive controller, it is noticing that $c(\partial M_u)$ and $c(\partial M_{u+\varepsilon})$. Generally, a good choice of $\mathcal{P}(\mathbf{u}_{ij})$ is an hypersphere $\mathcal{P}(\mathbf{u}_{i_j})=\mathbf{u}_{i_j}^T\mathbf{u}_{i_j}-M_0^2-\varepsilon\leq 0$, with $M_0 > \varepsilon > 0$.

5. Performance and stability of the dominant vehicle dynamics

Let us consider the path tracking problem for the time-varying dynamics of the vehicle and its solution by the adaptive control system described previously. First, let us assume that the thruster dynamics can be neglected, not yet its static characteristic. The actuator parasitics will be considered in the next section. We introduce here the analysis of convergence of tracking error trajectories for the adaptively controlled time-varying dynamics in three steps, namely for system parameters varying: 1) in continuous form, 2) in piecewise-constant form and 3) in piecewise-continuous form. These results are stated by theorems.

5.1 Asymptotic performance

Theorem I *(Asymptotic convergence for time-varying dynamics in continuous form)*
Consider the vehicle system (24)-(25), with bounded, piecewise continuous parameters M, C_{ci}, D_l, D_{qi}, B_1 *and* B_2, *and rates* $\dot{M}, \dot{C}_{ci}, \dot{D}_l, \dot{D}_{qi}, \dot{B}_1, \dot{B}_2 \in \mathcal{L}_1 \cap \mathcal{L}_\infty$ *or* $\mathcal{L}_2 \cap \mathcal{L}_\infty$. *Let moreover* $\boldsymbol{\tau}_t$ *in (63) generated by the direct adaptive controller (72)-(78) with the dynamic projection (79). Assume the thrusters are only described by their nonlinear characteristic in (46). Then, for every initial condition* $\boldsymbol{\eta}(t_0) \in \mathcal{S}_\eta$ *and* $\mathbf{v}(t_0) \in \mathcal{S}_v$, *the path tracking problem for given smooth reference trajectories* $\boldsymbol{\eta}_r(t)$ *and* $\mathbf{v}_r(t)$ *is achieved asymptotically with null error and the boundness of all variables of the adaptive control loop is ensured if the condition* $\boldsymbol{\eta}(t) \in \mathcal{S}_\eta$ *is fulfilled for all* $t \geq t_0$.

Proof:
Invoking the fact $\boldsymbol{\eta} \in \mathcal{S}_\eta$, *eventual singularities of* $J(\boldsymbol{\eta})$ *are avoided and a Lipschitz condition is guaranteed for the right member of the ODE system (24)-(25) in* $\mathcal{S}_\eta \times \mathcal{S}_v$. *Then it is assumed the existence and uniqueness of solutions* $\boldsymbol{\eta}(t)$ *and* $\mathbf{v}(t)$ *for* $t \in [t_0, \infty]$ *and arbitrary initial conditions given in the domain of attraction.*
Now, let us consider Q in (59) and the following candidate of Lyapunov function

$$V(t,\widetilde{\boldsymbol{\eta}},\widetilde{\mathbf{v}},U_i) = Q\left(t,\widetilde{\boldsymbol{\eta}},\widetilde{\mathbf{v}}\right) + Q_1(U_i - U_i^*) \tag{81}$$

where

$$Q_1(U_i - U_i^*) = \frac{1}{2}\sum_{i=1}^{17}\sum_{j=1}^{6}(\mathbf{u}_{i_j}-\mathbf{u}_{i_j}^*)^T\Gamma_i^{-1}(\mathbf{u}_{i_j}-\mathbf{u}_{i_j}^*) \tag{82}$$

and $\mathbf{u}_{ij}$ *is the column vector j of* $\mathbf{U}_i$, *and analogously,* $\mathbf{u}_{ij}^*$ *is the column vector j of the matrix* U_i^* *in (64)-(70). Then, taking the first derivative of V along the error trajectories* $\widetilde{\boldsymbol{\eta}}(t)$ *and* $\widetilde{\mathbf{v}}(t)$ *in* $t \in [t_0, \infty)$ *and since* $\boldsymbol{\eta} \in \mathcal{S}_\eta$, *one accomplishes*

$$\begin{aligned}\dot{V}\left(t,\widetilde{\boldsymbol{\eta}},\widetilde{\mathbf{v}},U_i\right) &= \dot{Q}\left(t,\widetilde{\boldsymbol{\eta}},\widetilde{\mathbf{v}},U_i\right) + \\ &+\sum_{i=1}^{17}\sum_{j=1}^{6}((\mathbf{u}_{i_j}-\mathbf{u}_{i_j}^*(t))^T\Gamma_i^{-1}\dot{\mathbf{u}}_{i_j} - (\mathbf{u}_{i_j}-\mathbf{u}_{i_j}^*(t))^T\Gamma_i^{-1}\dot{\mathbf{u}}_{i_j}^*(t)),\end{aligned} \tag{83}$$

where $\dot{Q}$ *is obtained for the control loop by replacing (63) in (61) for* $t \in [t_0, \infty)$

$$\begin{aligned}\dot{Q}(t,\tilde{\boldsymbol{\eta}},\tilde{\mathbf{v}},U_i) = &-\tilde{\boldsymbol{\eta}}^T K_p \tilde{\boldsymbol{\eta}} - \tilde{\mathbf{v}}^T K_v \tilde{\mathbf{v}} - \\ &-\tilde{\mathbf{v}}^T \sum_{i=1}^{6} \left(C_{c_i}(t) - U_{i\cdot} \times C_{v_i}(v_i)\right) \mathbf{v} - \tilde{\mathbf{v}}^T \left(D_l(t) + \frac{\dot{M}_c(t)}{2} - U_7\right) \mathbf{v} - \\ &-\tilde{\mathbf{v}}^T \sum_{i=1}^{6} \left(D_{q_i}(t) - U_{i+7}\right) |v_i| \mathbf{v} - \tilde{\mathbf{v}}^T \left(B_1(t) - U_{14}\right) \mathbf{g}_1 + \left(B_2(t) - U_{15}\right) \mathbf{g}_2 - \\ &-\tilde{\mathbf{v}}^T \left(M(t) - U_{16}\right) \mathbf{d} + \tilde{\mathbf{v}}^T \left(\frac{\dot{M}_c(t)}{2} + U_{17}\right) \tilde{\mathbf{v}} \,.\end{aligned} \tag{84}$$

Since $\dot{Q}(\mathbf{U}_i)$ *is globally convex in any convex set of the controller parameter space, it is valid*

$$\dot{Q}(\tilde{\boldsymbol{\eta}},\tilde{\mathbf{v}},U_i) - \dot{Q}(\tilde{\boldsymbol{\eta}},\tilde{\mathbf{v}},U_i^*(t)) \leq \sum_{i=1}^{17}\sum_{j=1}^{6} (\mathbf{u}_{i_j}^*(t) - \mathbf{u}_{i_j})^T \frac{\partial \dot{Q}}{\partial \mathbf{u}_{i_j}}, \tag{85}$$

for $t \in [t_0, \infty)$ *and subject to* $\boldsymbol{\eta} \in \mathcal{S}_\eta$. *Replacing (64)-(70) in (84) one obtains* $\dot{Q}(\tilde{\boldsymbol{\eta}},\tilde{\mathbf{v}},U_i^*) = -\tilde{\boldsymbol{\eta}}^T K_p \tilde{\boldsymbol{\eta}} - \tilde{\mathbf{v}}^T K_v \tilde{\mathbf{v}}$.

Now using (85) together with the projected adaptive laws $\dot{\mathbf{u}}_{i_j} = Proy\left(-\left(\Gamma_i \frac{\partial \dot{Q}}{\partial U_i}\right)_j\right)$ *deduced from (72)-(78) with (79), the function (83) can be bounded on the right by*

$$\dot{V}\left(t,\tilde{\boldsymbol{\eta}},\tilde{\mathbf{v}},U_i\right) \leq -\tilde{\boldsymbol{\eta}}^T K_p \tilde{\boldsymbol{\eta}} - \tilde{\mathbf{v}}^T K_v \tilde{\mathbf{v}} - \sum_{i=1}^{17}\sum_{j=1}^{6} (\mathbf{u}_{i_j} - \mathbf{u}_{i_j}^*(t))^T \Gamma_i^{-1} \dot{\mathbf{u}}_{i_j}^*(t). \tag{86}$$

Using the theorem statement that considers smooth parametric changes and considering (64)-(70), it is valid that $\dot{\mathbf{u}}_{i_j}^*(t)$ *does exist, and that is uniformly continuous and satisfy* $\dot{\mathbf{u}}_{i_j}^* \in \mathcal{L}_1 \cap \mathcal{L}_\infty$ *(and/or* $\dot{\mathbf{u}}_{i_j}^* \in \mathcal{L}_2 \cap \mathcal{L}_\infty$*). Then* $\dot{\mathbf{u}}_{i_j}^* \to 0$ *for* $t \to \infty$ *in* $t \in [t_0, \infty)$ *(see Ioannou & Sun, 1996, Lemma 3.2.5, pp. 76). On the other side, it is valid* $\dot{\mathbf{u}}_{i_j}^* \in \mathcal{L}_\infty$. *Then the projected adaptive law (79) ensures that all* $\mathbf{u}_{i_j}$ *be bounded in* $t \in [t_0, \infty)$. *Finally, integrating (86) with all these suppositions, one achieves*

$$\lim_{t\to\infty} \int_{t_0}^{t} \left(-\tilde{\boldsymbol{\eta}}^T K_p \tilde{\boldsymbol{\eta}} - \tilde{\mathbf{v}} K_v \tilde{\mathbf{v}}\right) d\tau \quad \leq \quad \lim_{t\to\infty} \int_{t_0}^{t} -c(\tau) Q\left(\tau,\tilde{\boldsymbol{\eta}},\tilde{\mathbf{v}}\right) d\tau \leq \tag{87}$$

$$\leq \quad \lim_{t\to\infty} - c_0 \int_{t_0}^{t} Q\left(\tau,\tilde{\boldsymbol{\eta}},\tilde{\mathbf{v}}\right) d\tau < \infty, \tag{88}$$

where c(t) and c_0 *are positive real values satisfying*

$$c(t) \quad = \quad \frac{\max\limits_{j=1,..,6} \{\lambda_j(K_p), \lambda_j(K_v)\}}{\max\limits_{j=1,..,6} \{\lambda_j(I/2), \lambda_j(M_c(t)/2)\}} \tag{89}$$

$$c_0 \quad = \quad \sup_{t \in \mathcal{S}_t \setminus [0,t_0)} c(t), \tag{90}$$

with $\lambda_j(.)$ *representing the eigenvalue j of the matrix indicated in parenthesis. Using the Lemma of Barbalat (Ioannou & Sun, 1996), it follows* $\lim_{t\to\infty}(\boldsymbol{\eta}(t)-\boldsymbol{\eta}_r(t)) = \mathbf{0}$. *In consequence, with (56) it is also valid*

$$\lim_{t\to\infty}(\mathbf{v}-J^{-1}(\boldsymbol{\eta})\dot{\boldsymbol{\eta}}_r) = \lim_{t\to\infty}(\mathbf{v}-J^{-1}(\boldsymbol{\eta}_r)\dot{\boldsymbol{\eta}}_r) = \lim_{t\to\infty}(\mathbf{v}-\mathbf{v}_r) = \mathbf{0}. \tag{91}$$

This proves that the path errors go to zero asymptotically as stated in the theorem.
For proving that the $\mathbf{U}_i$*'s are bounded, one employes (88), (59) and (62) together with the fact that* M, $\boldsymbol{\eta}$, $\mathbf{v}$, $\widetilde{\boldsymbol{\eta}}$ *and* J *are bounded. Moreover it is valid* $\lim_{t\to\infty}\dot{M}, \dot{C}_{c_1}, ..., \dot{C}_{c_6}, \dot{D}_l, \dot{D}_{q_1}, ..., \dot{D}_{q6}, \dot{B}_1, \dot{B}_2 = 0.$ *So one yields first* $\int_{t_0}^{\infty}\left|\widetilde{\mathbf{v}}\right|^2 d\tau < \infty$ *and* $\int_{t_0}^{\infty}\left|\widetilde{\mathbf{v}}\right| d\tau < \infty$. *Then, from (72)-(77) one obtains*

$$|U_i| \leq c_i \int_{t_0}^{\infty}\left|\widetilde{\mathbf{v}}\right| d\tau < \infty, \text{ for some constant } c_i > 0. \tag{92}$$

Similarly, from (78) it is valid

$$|U_{17}| \leq c_{17} \int_{t_0}^{\infty}\left|\widetilde{\mathbf{v}}\right|^2 d\tau < \infty, \text{ for some constant } c_{17} > 0, \tag{93}$$

and in this way it is concluded that the matrices $\mathbf{U}_i$*'s are also bounded. Finally, the boundness of* $\boldsymbol{\tau}_c$ *in (63) is demonstrated from the boundness of* $\widetilde{\boldsymbol{\eta}}$ *and* $\widetilde{\mathbf{v}}$, $\mathbf{d}$ *in (62),* J *and the proved boundness of the* $\mathbf{U}_i$*'s.* ■

Teorema II *(Asymptotic convergence for piecewise-constant time-varying dynamics)*
Let the statement of Theorem I be valid with the difference that the physical system matrices M, C_{c_i}, B_1 *and* B_2 *are constant for all* $t \in [t_0, \infty) / \mathcal{S}_{t_k}$ *and that they have finite changes for a finite sequence of isolated time points* $t_k \in \mathcal{S}_{t_k}$ *with* $k = 1, ..., n$, *while the system matrices* D_l *and* D_{q_i} *are constant. Then, for every initial condition* $\boldsymbol{\eta}(t_0) \in \mathcal{S}_\eta$ *and* $\mathbf{v}(t_0) \in \mathcal{S}_v$, *the path tracking problem for given smooth reference trajectories* $\boldsymbol{\eta}_r(t)$ *and* $\mathbf{v}_r(t)$ *is achieved asymptotically with null error and additionally the boundness of all variables of the adaptive control loop is ensured if the condition* $\boldsymbol{\eta}(t) \in \mathcal{S}_\eta$ *is fulfilled for all* $t \geq t_0$.

Proof:
As $\dot{Q}(t)$ *in (84) is continuous within* $[t_{k-1}, t_k)$ *with* $k = 1, ..., n$ *and additionally in the period* $[t_n, \infty)$, *and that* $\boldsymbol{\eta}(t) \in \mathcal{S}_\eta$, *it is valid (see (86) with constant matrices in (64)-(69) and* U_{17}^*=0, *Theorem I)*

$$\dot{V}(\widetilde{\boldsymbol{\eta}},\widetilde{\mathbf{v}},U_i) \leq -\widetilde{\boldsymbol{\eta}}^T K_p \widetilde{\boldsymbol{\eta}} - \widetilde{\mathbf{v}}^T K_v \widetilde{\mathbf{v}} < \infty, \tag{94}$$

for $t \in [t_{k-k}, t_k)$ *and* $t \in [t_n, \infty)$. *Employing the solution* $\mathbf{v}(t)$ *in* $[t_{n-1}, t_n)$ *and according to (43) and (56) one obtains*

$$\widetilde{\mathbf{v}}(t_n) = (I+\frac{1}{2}M^{-1}(t_n)\Delta M_n)\lim_{t\to t_n}\mathbf{v}(t)-J^{-1}(\boldsymbol{\eta}(t_n))\dot{\boldsymbol{\eta}}_r(t_n)+J^{-1}(\boldsymbol{\eta}(t_n))K_p\widetilde{\boldsymbol{\eta}}(t_n) \in \mathcal{S}_v. \tag{95}$$

Since $\breve{\boldsymbol{\eta}}(t_n)$ *and* $\breve{\mathbf{v}}(t_n)$ *are in the attraction domain of the error system in the ODEs, it yields*

$$\lim_{t\to\infty}\int_{t_n}^{t}\dot{V}(\tilde{\boldsymbol{\eta}},\tilde{\mathbf{v}},U_i)d\tau \le \lim_{t\to\infty} -c_0\int_{t_n}^{t} Q\left(\tilde{\boldsymbol{\eta}},\tilde{\mathbf{v}}\right)d\tau < \infty, \tag{96}$$

and by Lemma of Barbalat $\lim_{t\to\infty} Q = 0$ *and consequently also the errors* $\breve{\mathbf{v}}$ *and* $\breve{\boldsymbol{\eta}}$ *tend asymptotically to zero.*

To demonstrate the boundness of $\mathbf{U}_i$*, one notes first that the solutions* $\breve{\boldsymbol{\eta}}$ *are uniformly continuous while the solutions* $\breve{\mathbf{v}}$ *are only bounded in* $t < t_n$*. Thus, it is valid* $\int_{t_0}^{t_n}\left|\tilde{\mathbf{v}}\right|dt < \infty$ *and* $\int_{t_0}^{t_n}\left|\tilde{\mathbf{v}}\right|^2 dt < \infty$*, resulting* $|\mathbf{U}_i| < \infty$ *in this period. Then, from* $t_n < \infty$ *in advance, both solutions are bounded and continuous, and so the boundness of the matrices* $\mathbf{U}_i$*'s in* $[t_n, \infty]$ *is guaranteed. Finally,* τ_c *in (63) is also bounded as it can be deduced from the boundness of* $\breve{\boldsymbol{\eta}}$ *and* $\breve{\mathbf{v}}$*, of* $\mathbf{d}$ *in (62) and J together with the proved boundness of the* $\mathbf{U}_i$*'s.* ■

Corollary I *(Asymptotic convergence for staggered-continuous time-varying dynamics)*
Let the statement of Theorem I be valid with the difference that the physical system matrices M, C_{c_i}*, B1 and B2 are piecewise continuous and that Dl and* D_{q_i} *are continuous for all* $t \in [t, \infty]$*. The sudden bounded changes occur at* $t_k \in \mathcal{S}_{t_k}$ *with k = 1, ..., n. Additionally, all changes are* $\mathcal{L}_1 \cap \mathcal{L}_\infty$ *or* $\mathcal{L}_2 \cap \mathcal{L}_\infty$*. Then the asymptotic convergence of the tracking errors and the boundness of the adaptive control variables are ensured if the condition* $\boldsymbol{\eta}(t) \in \mathcal{S}_\eta$ *is satisfied for all* $t \ge t_0$*.*

Proof:
The proof of this corollary rises directly from the combination of the results in Theorem I and II in intervals of continuity $[t_{k-1}, t_k)$ *and then, after the last step of the trajectory* $\breve{\mathbf{v}}(t)$*, by considering the asymptotic disappearance of the parameter variation.* ■

Now the static characteristic of the actuators in (46) is considered in the convergence analysis (see also Fig. 2). It is remembering from the end part of Section 3 that by neglected thruster dynamics it is valid $\mathbf{n} = \mathbf{n}_r$ and $\mathbf{f} = \mathbf{f}_{ideal}$.

Corollary II *(Asymptotic performance of the adaptive control with static thruster characteristic)*
The adaptive control system employed in the path tracking problem for time-varying dynamics with piecewice continuous system parameters preserves the asymptotic properties and the boundness of all variables in the control loop, when the thrusters are described by (46) and (52).

Proof:
As $\mathbf{v}(t)$ *is piecewise continuous, so are* $\mathbf{v}_a(t)$ *in (46),* $\tau_t(t)$ *and* $\mathbf{f}_{ideal}(t)$ *in (52). Thus, considering the static characteristic, it is deduced that by solving (46) for* $\mathbf{n}_r(t)$ *with* $\mathbf{f}_{ideal}(t)$ *and* $\mathbf{v}_a(t)$*, there may exist one or two solutions at* $t = t_k \in \mathcal{S}_{t_k}$*, each one producing a propulsion that fulfills* $\mathbf{f}_{ideal} - \mathbf{f} = 0$ *in all* $t > t_0$*. Therefore, adopting some criterion in the case of multiplicity of* $\mathbf{n}_r(t_k)$*, one obtains from the last instant* t_n *of sudden change in advance that* $\breve{\mathbf{v}}(t)$ *will evolve continuously from* $\breve{\mathbf{v}}(t_n)$ *to zero asymptotically when* $t\to\infty$*. Moreover, due to the dynamic projection, all variables in the adaptive control loop result bounded in the intervals of continuity and also at* t_k*, independent of the multiple solutions for* $\mathbf{n}_r(t_k)$ *and of the temporal variation rate of the parameters so long as they vanish in time.*
■

5.2 Transient performance

The last results has concerned the asymptotic performance of the adaptive control system. However, nothing could be concluded about the control performance in short terms, it is,

about how significant are the transients and how fast the guidance system can adapt the initial uncertainty as well as the temporary changes of the dynamics. Finally, in the focus of future analysis, there would be the rolls that ad-hoc design parameters in both the control loop (i.e., K_p and K_v) and in the adaptive loop (i.e., the Γ_i's) play in the control performance during adaptation transients. A powerful result is given in the following theorem.

Theorem III *(Transient performance of the adaptive control system)*

Let the statement of Corollary I be considered for a piecewise-continuous time-varying dynamics. Then, after an isolated sudden change of M in $t_1 \in \mathcal{S}_{t_k}$ *and depending on the rate laws of* $\dot{M}_c, \dot{C}_{c_j}, \dot{D}_l, \dot{D}_{q_j}, \dot{B}_1$ *and* $\dot{B}_2$*, there exists a time point* $t_t > t_1$ *such that, from this on, the adaptive control system with gains* K_p*,* K_v *and* Γ_i *that are selected sufficiently large, can track any smooth reference trajectories* $\boldsymbol{\eta}_r$ *and* $\mathbf{v}_r$ *with a path error energy that is lower than a certain arbitrarily small level* $\varepsilon > 0$*.*

Proof:

At $t_1 \in \mathcal{S}_{t_k}$*, the kinematic reference trajectory fulfills* $\mathbf{v}(t_k)=(I+\frac{M^{-1}}{2}(t_k)\Delta M_1)\lim_{t\to t_k}\mathbf{v}(t)$ *(see (43)). Take this vector value as initial condition for the next piece of trajectory of* $\mathbf{v}$ *and consider (86) for* $t > t_1$*. Then it yields*

$$\dot{V}\left(t,\tilde{\boldsymbol{\eta}},\tilde{\mathbf{v}},U_i\right) \leq -c_K(\left|\tilde{\boldsymbol{\eta}}\right|^2+\left|\tilde{\mathbf{v}}\right|^2)+c_\Gamma^{-1}\sum_{i=1}^{17}\sum_{j=1}^{6}|\mathbf{u}_{i_j}-\mathbf{u}_{i_j}^*(t)|\,|\dot{\mathbf{u}}_{i_j}^*(t)|. \tag{97}$$

with $c_K = \min_{j=1,..,6}\{\lambda_j(K_p),\lambda_j(K_v)\}$ *and* $c_\Gamma = \min_{j=1,..,6;\ i=1,...,17}\{\lambda_j(\Gamma_i)\}$*. As the vectors* $\dot{\mathbf{u}}_{i_j}^*(t) \in \mathcal{L}_1 \cap \mathcal{L}_\infty$ or $\mathcal{L}_2 \cap \mathcal{L}_\infty$*, then these start to decrease after expiring some period referred to as* T_{i_j}*. Thus, for a given* $\varepsilon > 0$ *arbitrarily small, there exists some instant* $t_t > \max_{i,j}(T_{i_j}) + t_1$*, certain minimum values of* c_K *and* c_Γ *from which on* $\dot{V}(t, \tilde{\boldsymbol{\eta}}, \tilde{\mathbf{v}}, U_i) < 0$ *and the previous inequality satisfies*

$$\varepsilon \geq \left|\tilde{\boldsymbol{\eta}}\right|^2+\left|\tilde{\mathbf{v}}\right|^2 > \frac{1}{c_K c_\Gamma}\sum_{i=1}^{17}\sum_{j=1}^{6}|\mathbf{u}_{i_j}-\mathbf{u}_{i_j}^*(t)|\,|\dot{\mathbf{u}}_{i_j}^*(t)|, \tag{98}$$

for $t \geq t_t$*. Clearly, this result is maintained for all* $t \geq t_t$ *if no new sudden change of M occurs any more.* ■

Corollary III *(Transient performance of the adaptive control with static thruster characteristic)*

The result of Theorem III is preserve if the dynamics model and its adaptive control involve actuators with a static characteristic according to (46) and (52).

Proof:

Since $\mathbf{f}$ - $\mathbf{f}_{ideal}$ *is identically zero for all* $t \geq t_0$*, the true propulsion of the vehicle can exactly be generated according to* $\boldsymbol{\tau}_t(t)$ *by the adaptive control system. So the same conditions of Theorem III are satisfy and the same results are valid for the energy of the path error.* ■

It is seen that the adaptive control system stresses the path tracking property by proper setup of the matrices Γ_i's, not only in the selftuning modus but also in the adaptation phase for time-varying dynamics. This can occur independently of the set of K_p and K_v, whose function is more related to the asymptotic control performance, it is when $|\dot{\mathbf{u}}_{i_j}^*(t)| = 0$.

Moreover, it is noticing that in absence of time-varying parameters the dynamic projection on the adaptive laws (79) does not alter the properties of the adaptive control system since

the terms $(\mathbf{u}_{i_j} - \mathbf{u}^*_{i_j}(t))^T \Gamma_i^{-1} \dot{\mathbf{u}}^*_{i_j}(t)$ in (86) are null. The reason for the particular employment of a projection with a smoothness property on the boundary is just the fact that by time-invariant dynamics the control action will result always smooth.

6. State/disturbance observer

The last part of this work concerns the inclusion of the thruster dynamics together with its static characteristic according to (46)-(51) to complete the vehicle dynamics.

By the computation of $\boldsymbol{\tau}_t$ (t) with a suitable selection of the design matrices K_p, K_v and Γ_i's, it is expected that the controlled vehicle response acquires a high performance in transient and steady states. However, as supposed previously, the thruster dynamics (51) has to be considered as long as this does not look as parasitics in comparison with the achievable closed-loop dynamics. There exist approaches to deal with the inclusion of the thruster dynamics in a servo-tracking control problem that takes $\mathbf{f}_{ideal}$ (or the related $\mathbf{n}$) as reference to be followed by $\mathbf{f}$ under certain restrictions or linearizations of the whole dynamics. A comparative analysis of common approaches is treated in Whitcomb et al., 1999, see also Da Cunha, et al., 1995. Though the existing solutions have experimentally proved to give some acceptable accuracy and robustness, they do not take full advantage of the thruster dynamics and its model structure to reach high performance.

In this work a different solution is aimed that employs the inverse dynamics of the thrusters. In this case, the calculated thrust $\mathbf{f}_{ideal}$ in (52) will be used to be input a state/disturbance observer embedded in the adaptive control system to finally estimate the reference $\mathbf{n}_r$ to the shaft rate vector of the actuators that asymptotically accomplishes the previous goal of null tracking errors stated in (53)-(54), see Fig. 3 for the proposed control approach.

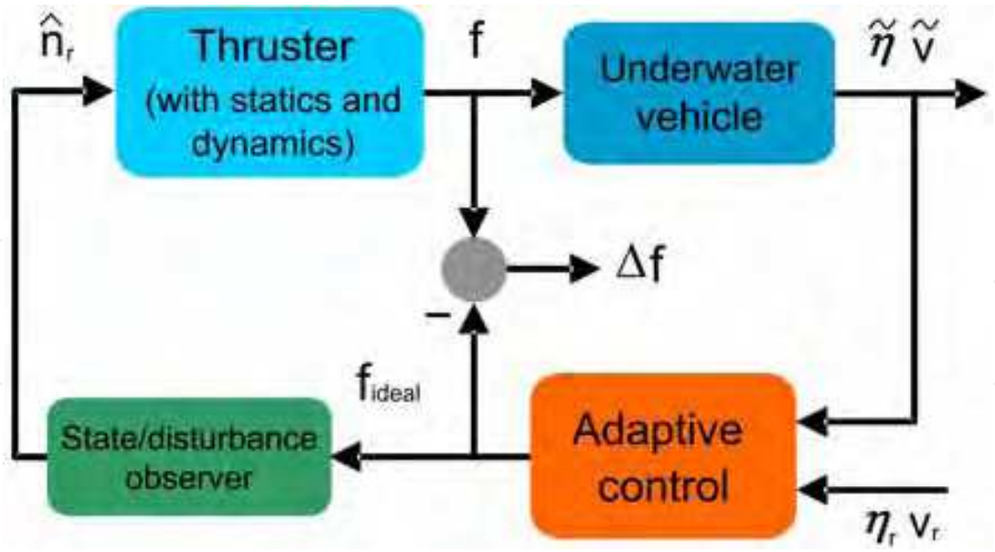

Fig. 3. Extended adaptive control system for the vehicle with thruster dynamics

As start point for an observer design, consider first one element of $G_2G_{PID}(s)$ in (49)- (50) corresponding to one thruster, and a state space description for this dynamics

$$\dot{\mathbf{x}} = A\mathbf{x} + \mathbf{b}(n_r - n) \tag{99}$$

$$n_2 \;=\; n - n_1 = \mathbf{c}^T\mathbf{x} \tag{100}$$

$$\bar{n}_2 \;=\; g_3(s)n - n_1 = -\left(1 - g_3(s)\right)n + \mathbf{c}^T\mathbf{x}, \tag{101}$$

with (A, **b**, **c**) a minimal set of a minimal description, x the state of this component and $g_3(s)$ a low pass filter to smooth sudden changes of n. Then, let

$$\dot{\hat{\mathbf{x}}} = A\hat{\mathbf{x}} + \mathbf{b}\,\hat{e}_c + \mathbf{k}_{n_2}(\bar{n}_2 - \hat{n}_2), \tag{102}$$

a differential equation for a state estimation x, with $\mathbf{k}_{n_2}$ a gain vector for the shaft rate error $\bar{n}_2 - \hat{n}_2$ and

$$\hat{n}_2 = \mathbf{c}^T\hat{\mathbf{x}} \tag{103}$$

$$\hat{e}_c = k_n\bar{n}_2 + k_{\dot{n}}\dot{\bar{n}}_2 + \mathbf{k}_{\hat{x}}^T\hat{\mathbf{x}}, \tag{104}$$

with $\hat{n}_2$ and $\hat{e}_c$ estimations of n_2 and of the thruster control error (n_r - n), respectively, and k_n, $k_{\dot{n}}$ and $\mathbf{k}_{\hat{x}}$ suitable gains for the components of $\hat{e}_c$. The function $\bar{n}_2$ and its first derivative $\dot{\bar{n}}_2$ can be deduced and calculated analytically from $\bar{n}_2 = g_3 n - n_1$ with $n_1 = g_1(s)\, f_{ideal}$ and (100). Also with (46) and Fig. 2 with $n^* = \frac{k_2}{2k_1}v_a$, it is valid

$$n = \operatorname{sign}(n - \frac{k_2}{2k_1}v_a)\sqrt{\frac{\operatorname{sign}(n) f_{ideal}}{k_1} + \left(\frac{k_2}{2k_1}v_a\right)^2} + \frac{k_2}{2k_1}v_a. \tag{105}$$

On the other side, with (99), (102), (103) and (101), the state error vector $\tilde{\mathbf{x}} = \mathbf{x} - \hat{\mathbf{x}}$ satisfies

$$\dot{\tilde{\mathbf{x}}} = (A - \mathbf{k}_{n_2}\mathbf{c}^T)\tilde{\mathbf{x}} + \mathbf{b}\,\tilde{e}_c + \mathbf{k}_{n_2}(1 - g_3(s))n, \tag{106}$$

with $\tilde{e}_c = (n_r - n) - \hat{e}_c$. Using (99)-(100) one gets

$$\dot{n}_2 = \mathbf{c}^T A\mathbf{x} + \mathbf{c}^T\mathbf{b}\,(n_r - n), \tag{107}$$

which combined with (104) and (101) it yields

$$\begin{aligned} \tilde{e}_c \;=\; & \left(1 - k_{\dot{n}}\mathbf{c}^T\mathbf{b}\right)(n_r - n) - \left(k_n\mathbf{c}^T + k_{\dot{n}}\mathbf{c}^T A\right)\mathbf{x} - \\ & - \mathbf{k}_{\hat{x}}^T\hat{\mathbf{x}} + \left(1 - g_3(s)\right)\left(k_n n + k_{\dot{n}}\dot{n}\right). \end{aligned} \tag{108}$$

It is noticed that there exist particular values of the gains $\mathbf{k}_{\hat{x}}$, k_n and $k_{\dot{n}}$ in (108) that fulfills

$$\begin{aligned} &\left(1 - k_{\dot{n}}\mathbf{c}^T\,\mathbf{b}\right) = 0 \\ &\mathbf{k}_{\hat{x}}^T = -\left(k_n\mathbf{c}^T + k_{\dot{n}}\mathbf{c}^T A\right). \end{aligned} \tag{109}$$

For the state space description in the observer canonical form one has $\mathbf{c}^T$ = [1, 0, ..., 0] and $\mathbf{b}^T$ = [$b_{m\text{-}1}$, ..., b_0]. Thus, with the thruster dynamics having a relative degree equal to one (i.e., $b_{m\text{-}1} \neq 0$), which is, on the other side, physically true, the observer conditions (109) turns into

$$k_{\dot{n}} = \frac{1}{b_{m-1}} \tag{110}$$

$$\mathbf{k}_{\hat{x}}^T = -\left[\frac{-a_{m-1}}{b_{m-1}} + k_n, \frac{1}{b_{m-1}}, 0, ..., 0\right], \tag{111}$$

with m the system order $G_2G_{PID}(s)$. With these values, (108) can be rewritten as

$$\tilde{e}_c = -\left(k_n \mathbf{c}^T + k_{\dot{n}} \mathbf{c}^T A\right)\tilde{\mathbf{x}} + \left(1 - g_3(s)\right)\left(k_n n + k_{\dot{n}} \dot{n}\right). \tag{112}$$

Additionally, combining (106) with (112) and the choice

$$\mathbf{k}_{n_2} = -k_n \mathbf{b}, \tag{113}$$

it yields

$$\dot{\tilde{\mathbf{x}}} = \left(I - k_{\dot{n}} \mathbf{b}\mathbf{c}^T\right) A\tilde{\mathbf{x}} + k_{\dot{n}} \mathbf{b}\left(1 - g_3(s)\right)\dot{n}, \tag{114}$$

where the matrix $\left(I - k_{\dot{n}} \mathbf{b}\mathbf{c}^T\right) A \leq 0$ with only one eigenvalue zero, while (1 - $g_3(s)$) is interpreted as a high-pass filter for the errors $\tilde{\mathbf{x}}$ and $\tilde{e}_c$ that are produced by fast changes of n in order to reach an effective tracking of f_{ideal}.

In order for (114) to give exponentially stable homogeneous solutions $\tilde{\mathbf{x}}(t)$, the first element of the initial condition vector $\hat{\mathbf{x}}(0)$ must be set to null. Moreover, it is noticing that only high-frequency components of $\dot{n}$ can excite the state error dynamics and that these avoid vanishing errors. So, the price to be be paid for including the thruster dynamics in the control approach is the appearance of the vector error $\Delta\mathbf{f}$ which is bounded and its magnitude depends just on the energy of the filtered $\dot{\mathbf{n}}$ in the band of high frequencies. According to (46), the influence of $\dot{\mathbf{n}}$ on $\Delta\mathbf{f}$ is attenuated by small values of the axial velocity of the actuators $\mathbf{v}_a$. In this way, the benefits in the control performance for including the thruster dynamics are significant larger than those of not to accomplish this, i.e., a vehicle model with dominant dynamics only.

Finally, the reference vector $\mathbf{n}_r$ for the inputs of all the thrusters is calculated by means of (104) and (105) in vector form as

$$\hat{\mathbf{n}}_r(t) = \hat{\mathbf{e}}_c(t) + G_3(s)\mathbf{n}(t). \tag{115}$$

The estimation of $\mathbf{n}_r$ closes the observer approach embedded in the extended structure of the adaptive control system described in Fig. 3.

7. Case study

To illustrate the performance of the adaptive guidance system presented in this Chapter, a case study is selected composed on one side of a real remotely teleoperated vehicle described in (Pinto, 1996, see also Fig. 1) and, on the other side, of a sampling mission application over the sea bottom with launch and return point from a mother ship. These results are obtained by numerical simulations.

7.1 Reference path

The geometric reference path $\boldsymbol{\eta}_r$ for the mission is shown in Fig. 4. The on-board guidance system has to conduct the vehicle uniformly from the launch point down 10(m) and to rotate about the vertical line $3/4\ \pi(rad)$ up to near the floor. Then, it has to advance straight 14(m) and to rotate again $\pi/4$ (rad) to the left before positioning correctly for a sampling operation. At this point, the vehicle performs the maneuver to approach 1(m) slant about $\pi/4$ (rad) to the bottom to take a mass of 0.5 (Kg), and it moves back till the previous position before the sampling maneuver. Afterwards it moves straight at a constant altitude, following the imperfections of the bottom (here supposed as a sine-curve profile). During this path the mass center G is perturbed periodically by the sloshing of the load. At this path end, the vehicle performs a new sampling maneuver taking again a mass of 0.5 (Kg). Finally the vehicle moves 1(m) sidewards to the left, rotates 3.535 (rad) to the left, slants up 0.289 (rad) and returns directly to the initial position of the mission. Moreover, the corners of the path are considered smoothed so that the high derivatives of $\boldsymbol{\eta}_r$ exist.

7.2 Design parameters

Here, the adaptive control system is applied according to the structure of the Fig. 3, i.e., with the vehicle dynamics in (24)-(25), the thruster dynamics in (46)-(50) and (52), the control law in (63), the adaptive laws in (72)-(78), and finally the estimation of the thruster shaft rate given in (115). The saturation values for the actuator thrust was set in $\pm 30N$.

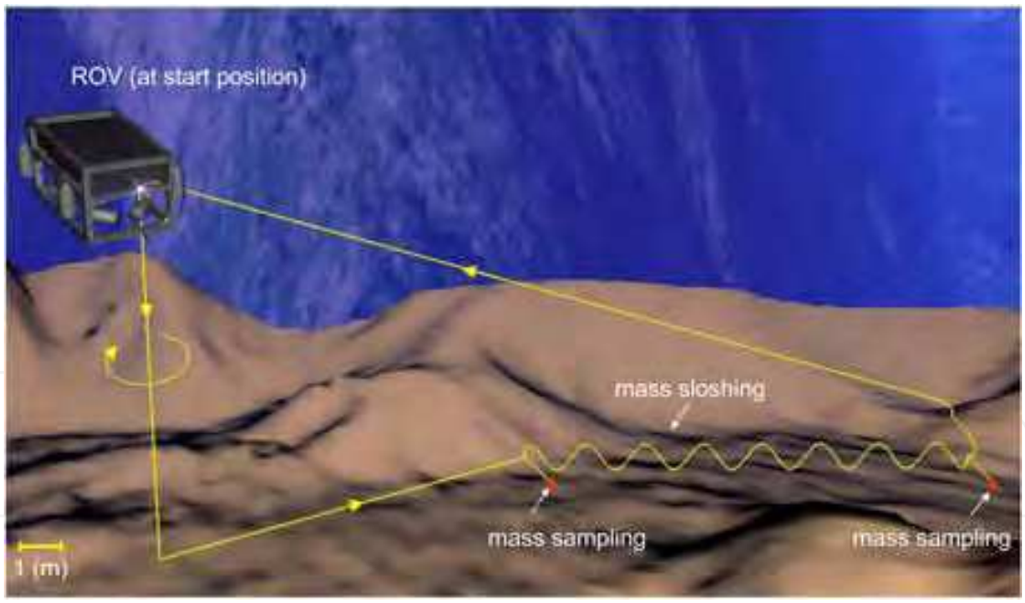

Fig. 4. Case study: sampling mission for an adaptively guided underwater vehicle

Moreover, the controller design gains are setup at large values according to theorem III in order to achieve a good all-round transient performance in the whole mission. These are

$$\begin{aligned} K_p &= \mathrm{diag}(1,1,1,1,1,1) \\ K_v &= \mathrm{diag}(10^3,10^3,10^3,10^3,10^3,10^3) \\ \Gamma_i &= \mathrm{diag}\left(10^2,10^2,10^2,10^2,10^2,10^2\right)\ \ i=1,...,16 \\ \Gamma_{17} &= \mathrm{diag}\left(1,1,1,1,1,1\right). \end{aligned} \tag{116}$$

Besides, the design parameters for the observer are setup at values

$$\begin{aligned} k_n &= 5 \times 10^{-3} \\ k_{\dot{n}} &= 13.005 \\ \mathbf{k}_{\hat{x}}^T &= [99.538, -13.005, 0] \\ \mathbf{k}_{n_2}^T &= \left[-3.844 \times 10^{-4}, -2.668, -0.207\right] \\ G_3(s) &= \operatorname{diag}\left(\tfrac{5\times 10^6}{(s+1000)(s+5000)}\right). \end{aligned} \tag{117}$$

The main design parameter k_n was chosen roughly in such a way that a low perturbation norm $\| \Delta\mathbf{f} \|_\infty$ in the path tracking and an acceptable rate in the vanishing of the error ($\mathbf{n}_r - \mathbf{n}$) occur. The remainder observer parameters $k_{\dot{n}}$, $\mathbf{k}_{\hat{x}}$ and $\mathbf{k}_{n_2}$ were deduced from the thruster coefficients and k_n according to (110), (111) and (113), respectively. Finally, the battery of filters $g_3(s)$ was selected with a structure like a second-order system.

7.3 Numerical simulations

Now we present simulation results of the evolutions of position and rate states in every mode. The vehicle starts from a position and orientation at rest at $t_0 = 0$ that differs from the earth-fixed coordinate systems in

$$\begin{aligned} &\Delta x(0) = 0.1(m) \quad \Delta y(0) = 0.1(m) \quad \Delta z(0) = 0.1(m) \\ &\Delta\varphi(0) = \tfrac{\pi}{6}(rad) \quad \Delta\theta(0) = \tfrac{\pi}{6}(rad) \quad \Delta\psi(0) = \tfrac{\pi}{4}(rad). \end{aligned} \tag{118}$$

Moreover, the controller matrices $U_i(0)$ are set to null, while no information of the system parameters was available for design aside from the thruster dynamics.

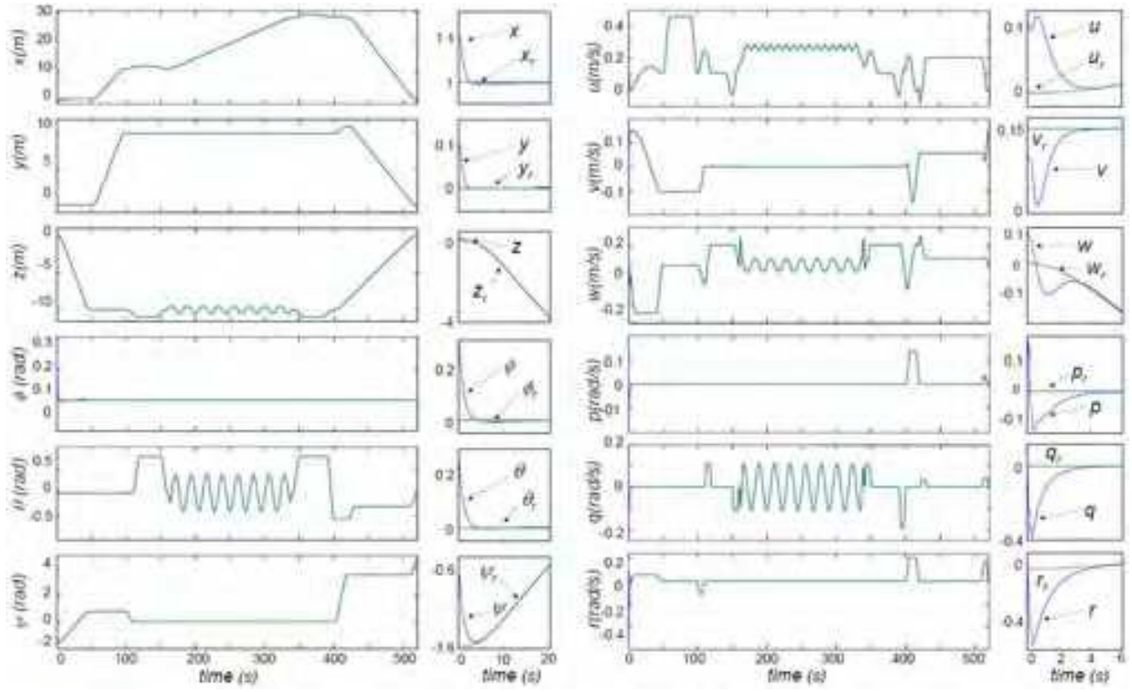

Fig. 5. Path tracking in the position modes ($\boldsymbol{\eta}$ vs. $\boldsymbol{\eta}_r$) (left) and in the kinematic modes ($\mathbf{v}$ vs. $\mathbf{v}_r$) (right)

In Fig. 5 the evolutions of position and kinematics modes are illustrated (left and right, respectively). One sees that no appreciable tracking error occurs during the mission aside from moderate and short transients of about 5(*s*) of duration in the start phase above all in the velocities. During the phase of periodic parameter changes (160 (*s*) up to 340 (*s*)) and at the mass sampling points occurring at 130 (*s*) and 370.5 (*s*), no appreciable disturbance of the tracking errors was noticed. However in the kinematics, insignificant staggered changes were observed at these points and a rapid dissipation of the error energy took place.
The sensibility of time-varying changes in the vehicle dynamics can be perceived above all in the thrust evolution. We reproduce in Fig. 6 the behavior of the eight thrusters of the ROV during the sampling mission; first the four vertical thrusts (2 and 3 in the bow, 1 and 4 in the stern) followed by the four horizontal ones (6 and 7 in the bow, 5 and 8 in the stern) (See Fig. 1). Both the elements of $\mathbf{f}_{ideal}$ and the ones of $\mathbf{f}$ are depicted together (see Fig. 6). It is noticing that almost all the time they are coincident and no saturation occurs in the whole mission time. Aside from the short transients of about 5(*s*) at the start phase, there is, however, very short periods of non coincidence between f and f_{ideal}. For instance, a transient at about 10(s) in the vertical thruster 3 occurs, where a separation in the form of an oscillation of (f - f_{ideal}) less than 4% of the full thrust range is observed (see f_3 and n_3 in Fig. 7, top). This is caused by jumps of the respective shaft rate by crossing discontinuity points around zero of the nonlinear characteristic.

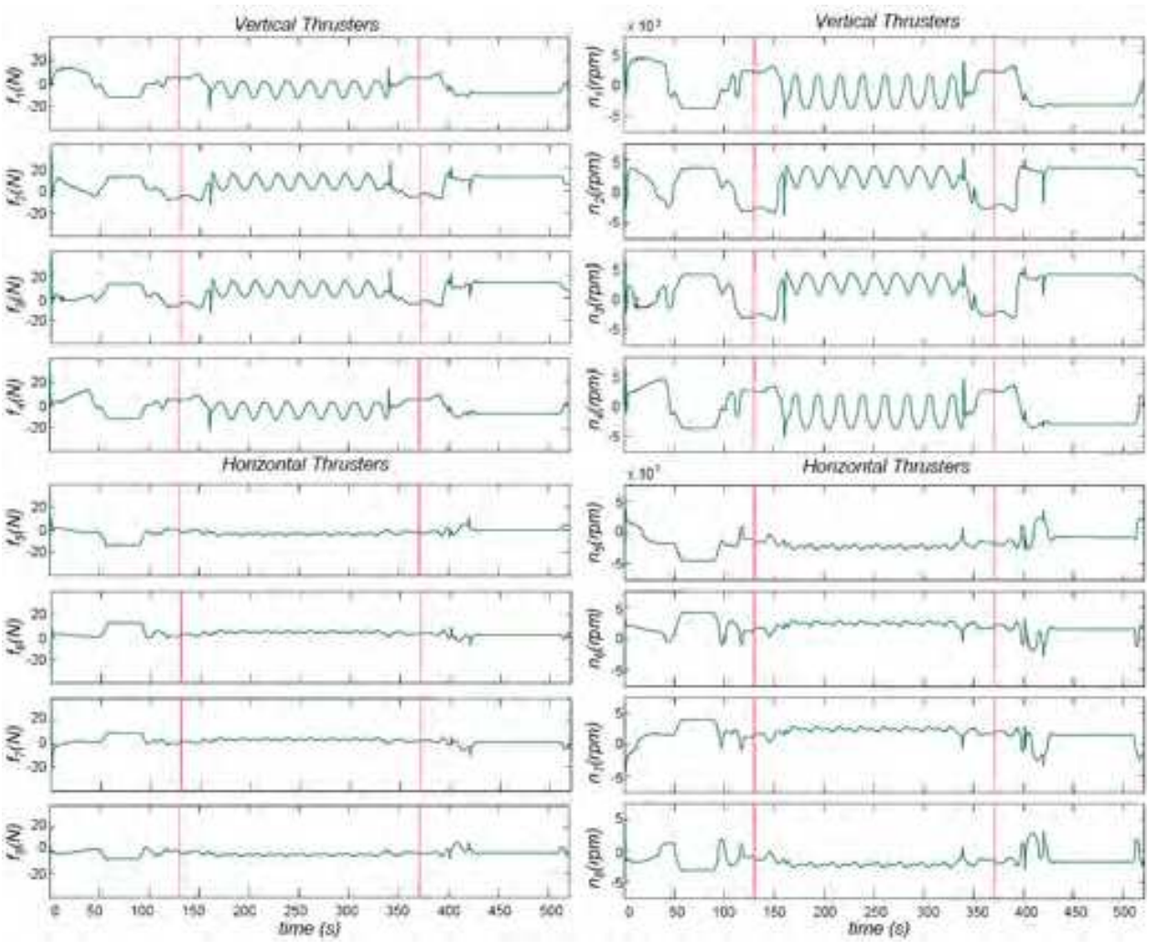

Fig. 6. Evolution of the actuator trusts ($\mathbf{f}$) (left) and shaft rates ($\mathbf{n}_t$ vs. $G_3\mathbf{n}_{ideal}$) (right)

Similarly, another short period with the same symptoms and causes takes place in the horizontal thruster 6 at about 404(*s*), also in the form of an oscillation with a separation less that 4% (see f_6 and n_6 in Fig. 7, bottom).

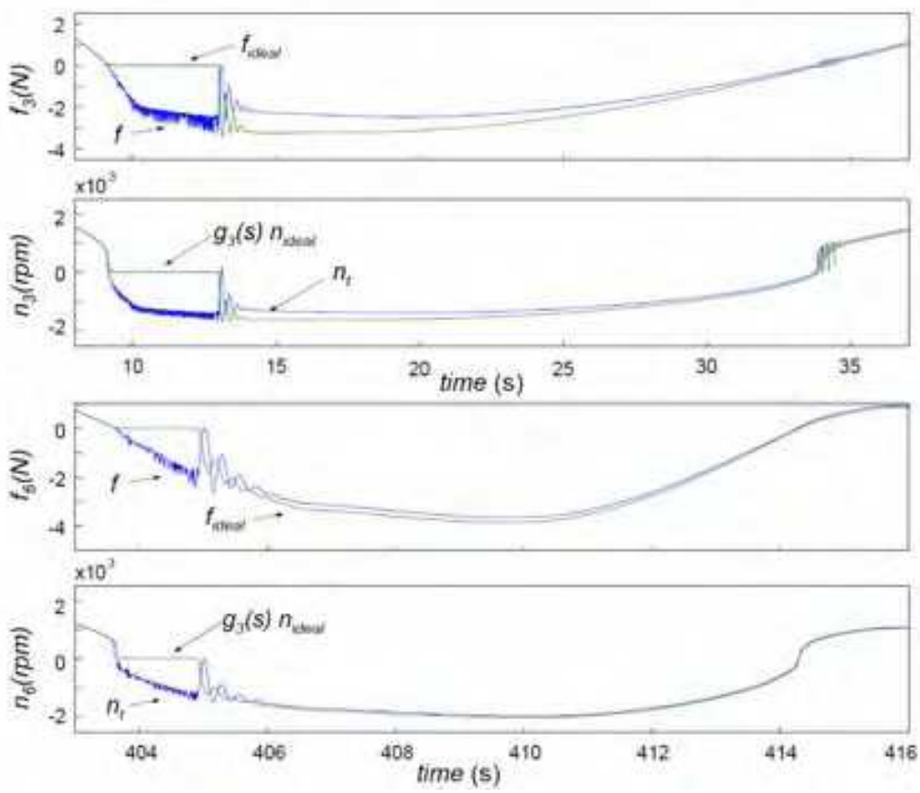

Fig. 7. Evolution of f vs. f_{ideal} and n vs. $g_3 n_{ideal}$ in thruster 3 at about 10(s) (top) and in thruster 6 at about 404(s) (bottom)

The sudden mass changes are absorbed above all by thrusters 2 and 3 (vertical thrusters in the bow) where jumps are also noticed in the evolutions of thrusts. However they have retained an exact coincidence between f and f_{ideal}. Jumps are noticed in all four horizontal thrusters too, with the same amplitude, however to a lesser degree. The coincidence between f and f_{ideal} also persists during periodic parameter changes in all thrusters, see Fig. 6, left.

The performance of the disturbance/state observer can be seen in Fig. 6, right, where the true shaft rate n versus the filtered ideal shaft rate $g_3 n_{ideal}$ are depicted for all thrusters. One notices a good concordance between both evolutions in almost the whole period of the mission. Contrary to the thrust evolutions, the convergence transients of n to $g_3 n_{ideal}$ at the start phase take a very short time less than 1(*s*). However, the evolutions begin with strong excursions and remain in time only a few seconds.

Similarly as in the thrusts f and f_{ideal}, there exist additionally two significant periods with short transients of non coincidence between n and $g_3 n_{ideal}$. These occur at about 10(s) and 404(s) by thrusters 3 and 6, respectively (see Fig. 7, top and bottom). All of them are related to crosses around the zero value under a relatively large value of its axial velocity v_a (cf. Fig. 2). One notices that the evolution of n is more jagged than that of $g_3 n_{ideal}$ due to the discontinuities at the short transients and due to the fact that $g_3 n_{ideal}$ is a smoothed signal.

8. Conclusions

In this chapter a complete approach to design a high-performance adaptive control system for guidance of autonomous underwater vehicles in 6 degrees of freedom was presented. The approach is focused on a general time-varying dynamics with strong nonlinearities in the drag, Coriolis and centripetal forces, buoyancy and actuators. Also, the generally rapid dynamics of the actuators is here in the design not neglected and so a controller with a wide working band of frequencies is aimed.

The design is based on a adaptive speed-gradient algorithm and an state/disturbance observer in order to perform the servo-tracking problem for arbitrary kinematic and positioning references. It is shown that the adaptation capability of the adaptive control system is not only centered in a selftuning phase but also in the adaptation to time-varying dynamics as long as the rate of variation of the system parameter is vanishing in time. Moreover, bounded staggered changes of the system matrices are allowed in the dynamics.

By means of theorem results it was proved that the path-tracking control can achieve always asymptotically vanishing trajectory errors of complex smooth geometric and kinematic paths if the thruster set can be described through its nonlinear static characteristics, i.e., when its dynamics can be assumed parasitic in comparison with the dominant controlled vehicle dynamics and therefore neglected. This embraces the important case for instance of vehicles with large inertia and parsimonious movements. On the other side, when the actuators are completely modelled by statics and dynamics, an observer of the inverse dynamics of the actuators is needed in order to calculate the setpoint inputs to the thrusters. In this case, the asymptotic path tracking is generally lost, though the trajectory errors can be maintain sufficiently small by proper tuning of special ad-hoc high-pass filters. It is also shown, that the transient performance under time-varying dynamics can be setup appropriately and easily with the help of ad-hoc design matrices. In this way the adaptive control system can acquire high-performance guidance features.

A simulated case study based on a model of a real underwater vehicle illustrates the goodness of the presented approach.

9. References

Antonelli, G.; Caccavale, F. & Chiaverini, S. (2004). Adaptive tracking control of underwater vehicle-manipulator systems based on the virtual decomposition approach. *IEEE Trans. on Robotics and Automation*, Vol. 20, No. 3, June 2004, 594-602, ISSN: 1042-296X.

Conte, G. & Serrani, A. (1999). Robust Nonlinear Motion Control for AUVs. *IEEE Rob. and Autom. Mag.*,Vol. 6, No. 2, June 1999, 32-38, ISSN: 1070-9932.

Da Cunha, J.P.V.S; Costa R. R. & Hsu, L. (1995). Design of a High Performance Variable Structure Position Control of ROV's. *IEEE Journal Of Oceanic Engineering*, vol. 20, No. 1, January 1995, 42-55, ISSN: 0364-9059.

Do, K.D. &Pan, J. (2003), Robust and adaptive path following for underactuated autonomous underwater vehicles. *Proceedings of American Control Conference 2003,* pp. 1994- 1999, Denver, USA, 4-6 June 2003.

Do, K.D.; Pan, J. & Jiang, Z.P. (2004). Robust and adaptive path following for underactuated autonomous underwater vehicles. *Ocean Engineering*, Vol. 31, No. 16, November 2004, 1967-1997, ISSN: 0029-8018.

Fossen, T.I. (1994). *Guidance and Control of Ocean Vehicles,* John Wiley&Sons, ISBN: 0- 471-94113-1, Chichester, UK.

Fossen, T.I & Fjellstad, I.E. (1995). Robust adaptive control of underwater vehicles: A comparative study. *Proceedings of the 3rd IFAC Workshop on Control Applications in Marine Systems*, pp. 66-74, Trondheim, Norway, 10-12 May 1995.

Fradkov, A.L.; Miroshnik, I.V. & Nikiforov, V.O. (1999). *Nonlinear and adaptive control of complex systems*, Kluwer Academic Publishers, ISBN 0-7923-5892-9, Dordrecht, The Netherlands.

Healey, A.J.; Rock, S.M.; Cody, S.; Miles, D. & Brown, J.P. (1995). Toward an improved understanding of thruster dynamics for underwater vehicles. *IEEE Journal Of Oceanic Engineering*, vol. 20, No. 4, Oct. 1995, 354–361, ISSN: 0364-9059.

Hsu, L.; Costa, R.R.; Lizarralde, F. & Da Cunha, J.P.V.S. (2000). Dynamic positioning of remotely operated underwater vehicles. *IEEE Robotics & Automation Magazine*, Vol. 7, No. 3, Sept. 2000 pp. 21-31., ISSN: 1070-9932.

Ioannou, P.A. & Sun, J. (1996). *Robust adaptive control*. PTR Prentice-Hall, ISBN: 0-13- 439100-4, Upper Saddle River, New Jersey, USA.

Jordán, M.A. & Bustamante, J.L. (2006). A Speed-Gradient Adaptive Control with State/ Disturbance Observer for Autonomous Subaquatic Vehicles. *Proceedings of IEEE 45th Conference on Decision and Control*, pp. 2008-2013, San Diego USA, 13-15 Dec. 2006.

Jordán, M.A. & Bustamante, J.L. (2007). An adaptive control system for perturbed ROVs in discrete sampling missions with optimal-time characteristics. *Proceedings of IEEE 46th Conference on Decision and Control,* pp. 1300-1305, New Orleans, USA, 12- 14 Dec. 2007.

Jordán, M.A. & Bustamante, J.L. (2007). Oscillation control in teleoperated underwater vehicles subject to cable perturbations. *Proceedings of IEEE 46th Conference on Decision and Control,* pp. 3561-3566, New Orleans, USA, 12-14 Dec. 2007.

Kreuzer, E. & Pinto, F. (1996). Controlling the Position of a Remotely Operated Underwater Vehicle. *App. Math. & Comp.*, Vol, 78, No. 2, September 1996 , 175-185. ISSN: 0096-3003.

Krstić, M.; Kanellakopoulus, I. & Kokotović, P. (1995). *Nonlinear and adaptive control design*, John Wiley and Sons, Inc., ISBN 0-471-12732-9, New York, USA.

Li, J.-H.; Lee, P.-M. & Jun, B.-H. (2004). An adaptive nonlinear controller for diving motion of an AUV, *Proceedings of Ocean '04 - MTS/IEEE Techno-Ocean '04*, pp. 282- 287, Kobe, Japan, 9-12 Nov. 2004.

O'Reagan, D. (1997) *Existence theory for nonlinear ordinary differential equations. Mathematics and its Application*s. Kluwer Academic Publishers, ISBN 0–7923–4511–8, Dordrecht: The Netherlands.

Pinto F. (1996). Theoretische und Experimentelle Untersuchungen zur Sensorik und Regelung von Unterwasserfahrzeugen, Doctoral Thesis.

Pomet, J.-B. & Praly L. (1992). Adaptive Nonlinear Regulation: Estimation from the Lyapunov Equation, *IEEE Transactions On Automatic Control*, vol. 31, No. 6, June 1992, 729-740, ISSN: 1558-0865.

Smallwood D.A. & Whitcomb, L.L. (2003). Adaptive identification of dynamically positioned underwater robotic vehicles. *IEEE Trans. on Control Systems Technology*, Vol.11, No. 4, July 2003 , 505-515, ISSN: 1558-0865.

Smallwood, D.A. & Whitcomb, L.L. (2004). Model-based dynamic positioning of underwater robotic vehicles: theory and experiment. *IEEE Journal of Oceanic Engineering*, Vol. 29, No. 1, Jan. 2004, 169-186, ISSN: 0364-9059.

Vidyasagar, M. (1993). *Nonlinear Systems Analysis*, Prentice-Hall, ISBN:0-13-623463-1, Upper Saddle River, NJ, USA.

Wang, J.-S. & Lee, C.S.G. (2003). Self-adaptive recurrent neuro-fuzzy control of an autonomous underwater vehicle. *IEEE Trans. on Robotics and Automation*, Vol. 19, No. 2, April 2003, 283-295, ISSN: 1042-296X.

Whitcomb, L.L. & Yoerger, D.R. (1999). Development, comparison, and preliminary experimental validation of nonlinear dynamic thruster models, *IEEE Journal Of Oceanic Engineering*, Vol. 24, No. 4, Oct. 1999 , 481–494. ISSN: 0364-9059.

Underwater Vehicles

Edited by Alexander V. Inzartsev

ISBN 978-953-7619-49-7
Hard cover, 582 pages
Publisher InTech
Published online 01, January, 2009
Published in print edition January, 2009

For the latest twenty to thirty years, a significant number of AUVs has been created for the solving of wide spectrum of scientific and applied tasks of ocean development and research. For the short time period the AUVs have shown the efficiency at performance of complex search and inspection works and opened a number of new important applications. Initially the information about AUVs had mainly review-advertising character but now more attention is paid to practical achievements, problems and systems technologies. AUVs are losing their prototype status and have become a fully operational, reliable and effective tool and modern multi-purpose AUVs represent the new class of underwater robotic objects with inherent tasks and practical applications, particular features of technology, systems structure and functional properties.

InTech Europe
University Campus STeP Ri
Slavka Krautzeka 83/A
51000 Rijeka, Croatia
Phone: +385 (51) 770 447
Fax: +385 (51) 686 166
www.intechopen.com

InTech China
Unit 405, Office Block, Hotel Equatorial Shanghai
No.65, Yan An Road (West), Shanghai, 200040, China
中国上海市延安西路65号上海国际贵都大饭店办公楼405单元
Phone: +86-21-62489820
Fax: +86-21-62489821

IntechOpen